Experimental petrology constraints on the recycling of mafic cumulate: a focus on Cr-spinel from the Rum Eastern Layered Intrusion, Scotland

Julien Leuthold, Jonathan D. Blundy, Richard A. Brooker

Abstract:

Reactive liquid flow is a common process in layered intrusions and more generally in episodically refilled magma chambers. Interaction between newly injected melt and cumulates, or crystal mushes, perturbs the liquid line of descent of the melt and modifies mineral chemistry and texture. We present insights into the effects of assimilation of mafic cumulate rocks (gabbro, troctolite) by co-genetic Mg-rich basalt liquid using one-atmosphere, controlled-fO_2 phase equilibrium experiments on picritic parental liquid to the Rum layered intrusion, Scotland. For picrite-only experiments at fO_2=QFM, Cr-spinel (Cr# = Cr/[Cr + Al + Fe^{3+}] = 0.43; Fe# = Fe^{2+}/[Mg + Fe^{2+}] = 0.32) saturates at 1320°C, olivine (Fo_{88}) at ~1290°C, plagioclase (An_{77}) at 1200°C and clinopyroxene (Mg#: 0.81) at 1180°C. In melting experiments on picrite + gabbro mixtures, plagioclase (1230°C, An_{80}) and clinopyroxene (1200°C, Mg#: 0.85) saturation temperature and mode are increased significantly. Cr-spinel in these experiments has a distinctive, low Fe#. In melting experiments on picrite + troctolite mixtures, plagioclase (An_{86}) saturates at 1240°C and clinopyroxene (Mg#: 0.81) at 1170°C. Al-rich spinel crystallizes at high temperature (>1220°C) and becomes more Cr-rich upon cooling, reaching the highest Cr# = 0.47 at 1180°C (0.54 at QFM-1.2). The experimental results confirm that plagioclase and clinopyroxene stability plays a major role in determining the composition of coexisting spinel. Comparing our experimental results to the Rum Eastern Layered Intrusion, we propose a model for the precipitation of spinel from picrite-troctolite hybrid melt that is compatible with the observed olivine, plagioclase and clinopyroxene chemistry.

Introduction:

Magma chambers are built up incrementally by repeated injections of melt into a growing crustal reservoir (e.g. Saint-Blanquat et al., 2011; Leuthold et al., 2012). In open magmatic systems, successive recharge of hot melt rejuvenates and assimilates resident crystal mush and cumulates (Tronnes, 1990; Hildreth and Moorbath, 1988; Bédard and Hébert, 1998; Dungan and Davidson, 2004; Leuthold et al., 2014a, 2014b). This process plays a critical role in the construction of large magma chambers via accumulation of successive sills or dykes (Annen et al., 2006; Solano et al., 2012) and is responsible for modification of percolating melt composition and cumulate/crystal mush mineral chemistry, texture and abundance. Interaction between resident cumulate mush and newly injected liquid (*reactive liquid flow*, or *infiltration metasomatism*, as defined by Irvine, 1980) modify both the cumulate and the reactive liquid, changing their modal composition, chemistry and texture (Figure 1) (Leuthold et al., 2014a). O'Hara and Herzberg (2002) stated that despite its importance, the assimilation of mafic crystals/cumulates by mafic melts is frequently underestimated. The lack of mineralogical, chemical and isotopic contrast between reactants can make it difficult to detect and distinguish crystal-melt interaction from simple crystallisation. Nevertheless, modifications of mineral chemistry and texture and melt composition have been revealed by detailed studies of intrusive rocks in a variety of geodynamic settings (e.g. Hildreth and Moorbath 1988; Bédard and Hébert, 1998; Leuthold et al., 2014a, 2014b).

In this study, we will examine the consequences of *reactive liquid flow* on the newly injected hot liquid whose composition is modified by assimilation of co-genetic mafic crystal mush and cumulate (troctolite,

gabbro). We show that this has important consequences for the phase equilibria and chemistry, particularly spinel compositions. Spinels crystallize down temperature from the liquidus for a wide range of mafic magmas, in different tectonic environments (Roeder, 1994). Understanding Cr-spinel (chromite) petrogenesis is of particular importance in layered intrusions, where chromitites are associated with platinum group element (PGE) ore deposits (e.g. Power et al., 2000; Grieko et al., 2004; O'Driscoll et al., 2009a, Latypov et al., 2013). Chromitite formation has long been debated and several petrogenetic models exist (see Campbell and Murck, 1993; Naldrett et al., 2012), including: liquid immiscibility (McDonald, 1965), oxidation (Ulmer, 1969; Cameron and Desborough, 1969), pressure fluctuations (Lipin, 1993), and assimilation of silicic crustal rock by mafic magma (Irvine, 1975; Spandler et al., 2005). Studying ophiolites, Bédard and Hébert (1998) have demonstrated the formation of chromitite via assimilation of crustal pyroxenite and gabbro by picrite melt intrusion. However, the most widely accepted model involves Cr-spinel saturation by mixing and hybridization of a newly injected olivine-saturated magma with a cogenetic, differentiated, more siliceous melt (Irvine, 1977).

We will use the Rum Eastern Layered Intrusion (Scotland) as a case study. This shallow, open-system, layered intrusion shows some of the world's best examples of *reactive liquid flow* (Leuthold et al., 2014a). The hybridization model of Irvine (1977) was applied to the Rum Eastern Layered Intrusion chromitites layers by Young (1984). O'Driscoll et al. (2009b) proposed an alternative model for the same chromitite occurrences on Rum whereby new picritic liquid assimilated troctolite cumulate. We will run a series of experiments to test the effect of gabbro and troctolite assimilation on the picrite liquid line of descent. We have chosen to run our experiments at atmospheric pressure (0.1 MPa) because of the ease of controlling oxygen fugacity, a key magmatic variable, in a gas mixing furnaces and the very low emplacement pressure of the Rum Eastern Layered Intrusion. The present experiments allow us to evaluate different hypotheses regarding the origin of chromitites on Rum, but with application to other layered intrusions and spreading ridges.

The Rum Eastern Layered Intrusion:

The Paleogene Rum Igneous Complex is part of the British Tertiary Volcanic Province and the North Atlantic Igneous Province (Emeleus and Gyopari 1992; Bell and Williamson 2002), dated at 60.53 ± 0.08 Ma by Hamilton et al. (1998), and related to the proto-Iceland plume (Kent 1995; Saunders et al. 1997; Bell and Williamson 2002). The Complex was intruded along the unconformity between the Archaean Lewisian gneiss and the overlying Precambrian arkoses of the Torridonian Group, at a pressure of 15±5 MPa (Holness, 1999). It is a bimodal intrusive complex with an initial episode of felsic activity and subsequent emplacement of a layered ultramafic to mafic braided sill complex (Leuthold et al., 2014b) into a caldera (Emeleus, 1997). Successive replenishments by mafic magma have built alternating olivine-rich and plagioclase-rich cumulate layers (Appendix figure 1). The Eastern Layered Intrusion is composed of a 750m-thick cumulate pile, divided into 15 intrusive units (Appendix figure 2). Each unit is formed of *peridotite* (olivine-rich cumulate) overlain by plagioclase-bearing cumulate (troctolite, gabbro and poikilitic gabbro, in variable proportions; known collectively as *allivalite*). The sill complex was fed by new magma injections along the Central Zone fault originating from a magma source at a depth of several kilometres (Emeleus et al., 1996). The intrusive units were thought originally to have formed by fractionation of individual batches of olivine-phyric picrite melts (Brown, 1956; Upton et al., 2002). Later studies showed that many units are composite and formed from successive, relatively small batches of either picritic or basaltic magma (Renner and Palacz, 1987; Bédard et al., 1988;

Holness and Winpenny, 2009). The cumulates themselves were later intruded by picritic magma (Bédard et al., 1988). Thus the Rum Eastern Layered Intrusion is an excellent example of *reactive liquid flow processes* (Figure 1) in an open magmatic system. Some of the best evidence of partial melting of resident troctolite and gabbro rocks by intrusive picrite liquids and subsequent melt hybridization include: Cr-spinel-bearing anorthosite produced after picrite percolation through troctolite (O'Driscoll et al., 2009b, 2010); formation of poikilitic gabbro with clinopyroxene oikocrysts (ca. 1 cm across) formed in gabbro percolated by hybrid melt (Leuthold et al., 2014a); and bulk rock reversals in isotopic composition (Palacz and Tait, 1985). Some troctolite and peridotite might also be the products of such modifications, representing highly reacted cumulates (Leuthold et al., 2014a).

Methods:

Starting materials:

Starting materials consisted of finely ground rock powders from four samples of the Rum Eastern Layered Intrusion (Table 1): a near-primary olivine-phyric picritic dyke (B62/2; McClurg, 1982, unpublished PhD. thesis; Upton et al., 2002), a basaltic dyke (11JL33; Leuthold et al., 2014a), a gabbro (11JL27; Leuthold et al., 2014a) and a troctolite (11JL16, Leuthold et al., 2014a). B62/2 contains euhedral to subhedral olivine phenocrysts (~10 vol%, $Fo_{85.9\text{-}80.5}$) in a fine-grained matrix composed of granular olivine ($Fo_{78\text{-}75}$) + plagioclase ($An_{69\text{-}66}$) + clinopyroxene (Mg#[1] = 0.82-0.71) + magnetite, with minor amounts of amphibole, mica and Cr-spinel (Cr#[2] = 0.32-0.43). B62/2 has a mildly alkalic, high MgO (Mg#: 0.67) composition that is a close match to the inferred Rum parental liquid (Upton et al., 2002). B62/2 is thought to have originated from low-degree partial melting of a lherzolite source close to the garnet-spinel transition within the proto-Icelandic mantle plume, with minor subsequent crustal contamination. Recent Icelandic picrites have a similar composition to B62/2 (Hémond et al., 1993). Basaltic dyke starting material 11JL33 has a composition (Mg#: 0.51) very similar to those studied by Toplis and Carroll (1995) and Thy et al. (2006) in the context of the liquid line of descent of the Skaergaard layered intrusion (Greenland). 11JL33 is composed of normally zoned plagioclase ($An_{61\text{-}15}$), clinopyroxene (Mg# = 0.73 to 0.65), K-feldspar, magnetite with ilmenite exsolution (3 vol%), titanite, zircon, epidote, and chlorite. According to McClurg (1982, unpublished PhD. Thesis) and Upton et al. (2002) B62/2 picrite and 11JL33 basalt represent co-existing mafic end-member liquid compositions (Figure 2). A few picritic dykes at Rum (e.g. M9) have accumulated olivine and spinel macrocrysts crystallized in a near-Moho reservoir (Upton et al., 2002); these deeper intrusions were not considered experimentally but are discussed in terms of petrogenesis.

Partial melts of troctolite and gabbro co-existed with intrusive picrite (Leuthold et al., 2014a). To study experimentally the effect of mafic crystal assimilation into picrite, we used as starting material mechanical mixtures (hybrids) of picrite (B62/2) with gabbro (11JL27) and troctolite (11JL16). Gabbro 11JL27 is composed of 13 vol% olivine, 53 vol% plagioclase and 34 vol% clinopyroxene. Troctolite 11JL16 is composed of 26 vol% olivine, 0.2 vol% Cr-spinel, 70 vol% plagioclase and 4 vol% clinopyroxene (see Leuthold et al. [2014a] for details). The hybrid series of experiments is intended to evaluate the effect of variable proportions of mafic rock assimilation (0, 50 and 100%) on the reactive picrite liquid line of descent.

[1] Mg# = molar $Mg/[Mg + Fe^{2+} + Fe^{3+}]$

[2] Cr# = molar $Cr/[Cr + Al + Fe^{3+}]$

Experiments:

Experiments #27 to #109 were performed at the University of Bristol in GERO™ vertical furnaces at atmospheric pressure. We controlled the oxygen fugacity (fO_2) by employing mixed CO and CO_2 gases controlled by Alicat Scientific flow controllers. The fO_2 was measured before and after each experiment with SIRO2™ solid zirconia oxygen sensors. The temperature was monitored adjacent to the sample with a Type B thermocouple. Additional experiments (#110 to #173) were run at ETH Zurich using a similar GERO™ vertical furnaces with controlled fO_2 conditions by mixing CO_2 and H_2. Results from the two laboratories are mutually consistent.

The starting material powder was mixed with a small amount of ultrapure water, as a binder, and mounted on a thin Pt-Rh wire loop. Most individual mounts were initially melted at supraliquidus conditions and then quenched to a glass. In isothermal experiments, the crystal-free glass was taken directly to the desired temperature at fO_2 of QFM-2.2 to QFM+1.8[3] (see Appendix figure 2). In cooling-rate experiments, different cooling modes were used. In these experiments, we progressively ramped the temperature (<100°C/h), whilst adjusting fO_2. This method is very similar to that used by Fisk and Bence (1980). In both cases, we also used the temperature oscillation (±10°C) technique (Mills et al., 2011; Mills and Gardner, 2013) to grow coarse crystals. Following ramped cooling the sample was left to equilibrate typically for 5 to 15h and then drop-quenched into water. Crystals show no evidence of quench overgrowths and the quenched liquid is pure glass. High spatial resolution core-rim chemical profiles show no rim zoning between crystal pairs or with liquid. These observations are considered to indicate both equilibrium and effective quenching without re-equilibration or recrystallization (e.g. Sisson and Grove, 1993b). For comparison with fully molten starting material, we have also run a few melting experiments, where the starting material was equilibrated at a temperature below the liquidus. Additionally, we have also reacted picrite with troctolite. Samples were melted above the liquidus, quenched and equilibrated at 1250 and 1220°C at QFM-1.2 prior to juxtaposition and reaction for 2 to 18 hours. Experimental run conditions and products are given in the Tables 2 to 5, schematic cooling paths are presented in the Appendix figure 2, selected BSE images are shown in Figure 3 and mineral stability fields are presented in Figure 4.

Analyses:

Run products were mounted in EPOFIX™ resin blocks and polished to 1µm. We used the University of Bristol Hitachi S-3500N and the ETH Zürich Jeol JSM-6390 LA scanning electron microscopes (SEM), both equipped with Thermo Fisher Noran energy dispersive spectrometer (EDS x-ray detector), to acquire backscatter electron (BSE) images and characteristic X-ray maps at 20kV that were used to determine phase assemblages and proportions using *imageJ* software. Repeated analyses on the same samples provided an estimate of the uncertainties on mineral proportions, which were typically less than ±5 vol%. The Bristol JEOL 8530F FEG-EMPA operating at low voltage was required to measure accurately the major element composition of small phases, without contamination by fluorescence from the surrounding glass (Saunders et al., 2014). The operating conditions were 10kV, 10nA and a beam size of 0.1µm for crystals (spinel has a typical diameter of ~2 µm) and 5-10µm for glass. Natural and synthetic silicates and oxides were used as primary and secondary standards. The EMP analyses of the Pt-13Rh wire showed very limited Fe gain during short experiments (<1h) at high

[3] QFM: quartz-fayalite-magnetite equilibrium, corresponding to Ni-NiO-0.8 (NNO-0.8)

temperature (1260°C). After an extreme run duration of 60 hours at 1170°C and QFM conditions, the glass once remolten above the liquidus had only lost 1 wt% FeO_{tot} (10% relative). The glass Fe^{3+}/Fe_{tot} ratio was calculated using Kress and Carmichael (1991) algorithm at the experimental temperature and fO_2. Glass compositions in fully molten and subsequently re-equilibrated experiments and in partially molten powder are identical, but crystals are strongly zoned in the later and difficult to interpret. Thus, we have decided to focus on the results from fully molten starting materials. Analytical results are presented in Appendix table 1.

Liquid line of descent:

Phase proportions and compositions:

The mineral modes are given in Tables 2 to 5 and Figure 5; mineral compositions are given in Appendix table 1 and Figure 6. From 1160°C, the crystals form a connected framework in picrite experiments (46 vol% liquid).

Picritic dyke B62/2, considered as the most probable parental liquid for Rum (Leuthold et al., 2014a), has liquidus and solidus temperatures of 1320°C and 1110°C respectively (Figure 4). Olivine and Cr-spinel are the liquidus phases, plagioclase saturates at 1200°C and clinopyroxene at 1180°C (Figure 4 and Appendix figure 3). The liquid fraction strongly decreases once plagioclase and clinopyroxene saturate (Figure 5). Upon cooling, the B62/2 experimental glasses become basaltic and finally basanitic (Figure 2). Their compositions are identical to Iceland plume lavas (Hémond et al., 1993) (Figure 2). As expected, the olivine forsterite content is higher under more oxidized conditions.

Basalt 11JL33, which is similar in composition to other basaltic dykes on Rum (McClurg, 1982, unpublished PhD thesis) has a liquidus temperature of 1165°C, when olivine, spinel and plagioclase co-saturate (Figures 4, 5 and Appendix figure 3). The 11JL33 experiments corroborate the Toplis and Carroll (1995) and Thy et al. (2006) experiments with comparable saturation temperatures and modes for olivine, plagioclase and clinopyroxene.

Gabbro assimilation by picrite tends to reduce the liquidus and increase the solidus temperatures (Figures 4, 5). Olivine saturation is delayed in comparison to the picrite starting material and is modally less important, resulting in a higher Mg# at high melt fractions (Figures 2, 6), amplified by the low liquid FeO content. The glass is CaO- and Al_2O_3-enriched which increases plagioclase and clinopyroxene saturation temperatures (Figures 2, 4 and Appendix figure 3).

Troctolite assimilation increases the liquidus and solidus temperatures of picrite (Figures 4, 5), as well as the glass Al_2O_3 and MgO contents. The plagioclase, olivine and spinel saturation temperatures are all increased while clinopyroxene stability is decreased (Figures 4, 5).

Spinel

Crystals are typically euhedral and ~2um across. Only spinel in contact with glass was considered, to guarantee equilibration with melt during cooling-rate experiments. Cr-spinel Fe-Mg re-equilibration with melt is relatively rapid (Scowen et al., 1991); nevertheless core and rim analyses obtained by the FEG-EMPA reveal absence of any zoning that may be related to quenching. B62/2 picrite high temperature QFM crystals (1280°C), co-crystallizing with olivine, are Cr-rich (Cr# = 0.43, Al/(Al+Cr) = 0.53). From 1230-1200 to 1150°C the spinel Al/(Al+Cr) progressively decreases from 0.65 to 0.54 (Figure 7a). Upon further cooling along the QFM

equilibrium, the Fe^{3+} content strongly increases. At and below 1140°C, Fe-enrichment rapidly increases and magnetite becomes the stable spinel phase. Crystals in cooling-rate experiments have slightly higher Cr# and lower Fe#[4] than in isothermal experiments at the same temperature. The Fe# increases upon cooling (from 0.32 at 1280°C, to 0.78 at 1110°C), together with TiO_2 (Figure 7). Spinel is distinctly more abundant in oxidized experiments (~1 vol%) (Figure 3e). Conversely, it is rare and corroded in reduced (QFM-2.2) experiments (Figure 3f) and is absent in clinopyroxene-bearing runs. The Fe^{2+}/Fe^{3+} ratio of spinel is strongly affected by the fO_2, with higher Fe^{3+} content and Fe# under oxidized conditions (Figures 7a, 8c).

In the basaltic experiments, minor spinel (maximal Cr# = 0.46 at 1150°C, QFM) saturates at 1160°C. At 1090°C, abundant titanomagnetite crystallizes (7 vol%) and the liquid has a ferrogabbro composition (Figures 2 and 7b). Under reduced conditions, Cr-spinel and titanomagnetite co-exist.

Spinels in picrite-gabbro and gabbro experiments follow very similar trends. They have a slightly lower Al/(Cr+Al) and higher Fe# than the B62/2 picrite (Figure 7a) consistent with variation in starting compositions. The gabbro spinel Mg# and Cr# vary within a limited range. Noticeably, the Fe^{3+} does not increase from liquidus to solidus conditions (Figure 8).

Along the picrite-troctolite QFM liquid line of descent, Cr# increases from 0.11 (Al-spinel) to 0.48 (Cr-spinel) in the interval from 1230 (58 vol% melt) to 1190°C (28 vol% melt). Concomitantly, the Fe# strongly increases to 0.47 (Figure 7a, 8). At QFM-1.2, Cr# reaches a maximum value of 0.54 at 1180°C. At similar temperatures, the TiO_2 concentration is slightly higher in picrite-troctolite experiments compared to picrite experiments, despite the lower Ti-content of the starting material, most probably related to a lower melt fraction (Figure 7b). Spinel in the troctolite-only experiment at 1210°C (5 vol% liquid) is strongly Al-enriched (Al/[Al+Cr] = 0.98).

In picrite-troctolite experiment reacted for 5 hours at 1250°C, we observe a 200µm reaction rim with olivine and spinel at the interface between the two magmas (Figure 9). Upon longer reaction times, this rim disappears. The spinel modal abundance varies from 1.2 vol% in troctolite to 3.5 vol% in the inner part of the reaction rim to 0.1vol% in the picrite. The spinel chemistry spatially evolves from Al-spinel in troctolite to Cr-spinel in the picrite. The two extremes in composition are identical to the picrite and troctolite experiments equilibrated under similar conditions (Figure 8). At the same time, the liquid Al_2O_3 content decreases from 18.4 to 14.2 wt% and the Cr_2O_3 concentration increases from 0 to 0.13wt%.

Olivine

The olivine proportion in picrite experiments increases from 3 vol% at 1280°C to ~15 vol% at 1110°C (Figure 5). The forsterite (Fo) content varies very little until clinopyroxene saturation at 1180°C (Figure 6). At identical melt volume fraction, Fo is slightly higher in oxidized experiments due to reduction in Fe^{2+}/Fe^{3+} ratio in the coexisting melt. Olivine is zoned in cooling-rate experiments, especially when equilibrated at a low final temperature. However, rim composition are identical to olivine crystals in isothermal experiments. In the basaltic experiments, olivine saturates at 1160°C. The crystals have the lowest forsterite content (down to 0.54).

At identical temperatures, the olivine fraction is lower in picrite-gabbro (50-50 mix) and gabbro experiments (Figure 3d). Glass in picrite-gabbro and gabbro experiments is relatively Fe-depleted and the olivine forsterite content is, therefore, elevated compared to picrite experiments. At identical temperatures, the olivine fraction is

[4] Fe# = molar $Fe^{2+}/(Mg+Fe^{2+})$

higher for the picrite-troctolite 50-50 mix (Figure 3d), but the forsterite and NiO contents are indistinguishable from B62/2 liquids prior to clinopyroxene saturation.

Plagioclase

In the picritic experiments, plagioclase saturates at 1200°C (85 vol% melt) and modally increases to 45 vol% at 1110°C (4 vol% melt) (Figures 4, 5). The anorthite content regularly decreases while the Fe_2O_3 content linearly increases upon cooling at QFM. The fO_2 has no effect on the anorthite content, but plagioclase is more Fe-rich at more oxidized conditions, supporting prevalent incorporation of Fe^{3+} (Wilke and Behrens, 1999). Under reducing conditions, the Fe_2O_3 content decreases down-temperature. Crystals in cooling-rate experiments are unzoned and their chemistry is identical to plagioclase in isothermal runs.

In the basaltic liquid experiments, plagioclase is a liquidus phase, together with olivine and spinel, at 1160°C. The anorthite content extends the picrite plagioclase trend, down to An_{51}. The Fe_2O_3 progressively decreases during cooling, once titanomagnetite saturates.

In picrite-gabbro and gabbro experiments, the plagioclase saturation temperature increases to 1230°C and ~1240°C respectively. At similar temperature, the plagioclase anorthite content is higher than in pure picrite experiments (Figure 6). The Fe_2O_3 concentration is lower in hybrid liquid experiments.

In picrite-troctolite experiments, plagioclase saturates at ~1240°C and its modal abundance increases rapidly. At 1190°C (38 vol% melt), it amounts to ~36 vol%. The plagioclase anorthite content is higher than along the B62/2 picrite liquid line of descent (up to An_{86} in picrite-troctolite experiment at 1230°C) (Figure 6). The plagioclase Fe_2O_3 content in picrite-troctolite experiments is highly variable.

Clinopyroxene

For the picrite QFM line of descent, clinopyroxene saturates at 1180°C (68 vol% melt) and its proportion progressively increases to 30 vol% at 1110°C (Figures 4, 5). The clinopyroxene Al_2O_3 and Fe_2O_3 concentrations are distinctly higher and Cr, Fe^{2+} and Si contents are lower under oxidized conditions (Figure 6). TiO_2 increases constantly during cooling (not shown), from 0.8 to 2.2 wt%, regardless of fO_2.

In the basaltic liquid experiments, clinopyroxene saturates from 1120°C at QFM, but at 1150°C at QFM-0.7 and QFM-1.2. The Mg# and Cr_2O_3 (<0.3wt%) contents are the lowest of all experiments. The Al_2O_3 content shows a large scatter (Figure 6). TiO_2 increases from 1.1 to 2 wt% at 1085°C, before it drops to 0.9 at lower temperature, once titanomagnetite saturates.

In picrite-gabbro and gabbro experiments, the clinopyroxene saturation temperature is increased to ~1200°C and ~1220°C respectively. The clinopyroxene mode is highest along these liquid lines of descent and the Cr_2O_3 concentration is distinctly higher (up to 1.40 wt%) (Figure 6). As for olivine, the clinopyroxene Mg# is higher than in picrite experiments and the TiO_2 concentration is distinctly lower (increase from 0.1 to 1.3 wt%).

In picrite-troctolite experiments, clinopyroxene saturation is delayed until 1170°C. The Al_2O_3 and Cr_2O_3 concentrations are similar to those in the picrite experiments at QFM.

MELTS calculations:

It is instructive to compare our experimental results to those calculated using MELTS (Ghiorso and Sack, 1995; Asimow and Ghiorso, 1998). MELTS calculations were run using identical starting picritic and basaltic

liquid compositions and similar conditions to our experiments. Mineral modes and saturation temperatures appear to accurately reproduce our Rum liquid line of descent (Figure 5). The spinel, olivine, clinopyroxene and liquid compositions are also very similar (Figures 6, 8), but the predicted plagioclase anorthite content is systematically too low; clinopyroxene Cr_2O_3 content is not considered by MELTS (Cr is only incorporated into Cr-spinel). This comparison confirms that MELTS calculations can be used to estimate anhydrous basalt liquid and crystal compositions at low pressure. Hybrid melts experiments mineral saturation temperatures and modal abundances are also well reproduced by MELTS calculations.

As a first approximation, based on the observation that MELTS calculations are valid at our conditions, we have run additional MELTS calculations varying the pressure (up to 0.3 GPa), starting liquid composition (Rum picritic and basaltic dykes, picrite doped with 0.2 wt% Cr_2O_3, 50% plagioclase or 50% clinopyroxene crystals, troctolite or gabbro melt), oxygen fugacity (QFM+0.8 to QFM-2) and varying water content (anhydrous to 0.2 wt%), whlist considering both equilibrium and fractional crystallization. The various liquid lines of descent are presented in Figure 8b. Most calculations were run along a fixed oxygen buffer, which is consistent with the experiments, but not necessarily appropriate to natural systems. It is interesting to note that calculations where the fO_2 is left free to vary during crystallization from initially reduced conditions (QFM-1), produce a second Fe-rich, Si-poor low temperature liquid at the saturation point of whitlockite/apatite. Such an immiscible Fe-rich liquid has not been documented on Rum, but has been described from the Skaergaard and Sept Iles layered intrusions (Jakobsen et al., 2005; Charlier et al., 2011) and the British Tertiary Volcanic Province island of Mull (Kerr et al., 1999).

Case study: Cumulates of the Rum Eastern Layered Intrusion

Our experimental results can be used to evaluate magmatic evolution in the Rum Eastern Layered Intrusion. The Rum cumulate assemblage comprises olivine-rich gabbro (60-75 vol% olivine, 15-35 vol% plagioclase and <15 vol% clinopyroxene), troctolite (15-55 vol% olivine, 45-85 vol% plagioclase and <10 vol% clinopyroxene) and gabbro (5-20 vol% olivine, 50-60 vol% plagioclase and 20-50 vol% clinopyroxene) (Holness et al., 2007; Leuthold et al., 2014a). Poikilitic gabbro with clinopyroxene oikocrysts and Cr-spinel bearing anorthosite are also found. Along the profile F (see location on Appendix figure 1) sampled by Holness et al. (2007) across Units 8 and 9, the Unit 9 peridotite sill is absent and cumulates are mainly composed of texturally mature gabbro with olivine, plagioclase and clinopyroxene as liquidus phases. These are interpreted to be unmodified by subsequent reactive liquid flow processes (Holness et al., 2007). Leuthold et al. (2014) studied the Unit 9 in the profile M area, sampled by Sides (2008, unpublished PhD thesis), 400 m south of profile F.

Spinel:

At the Unit 7-8 and 11-12 boundaries, millimetre-thick chromitite seams occur at the interface between overlying olivine-rich feldspathic peridotite and underlying feldspar-rich allivalite (anorthosite, troctolite) (Dunham and Wadsworth, 1978 and references therein; O'Driscoll et al., 2009b, 2010). Spinel is frequently associated with plagioclase, either in anorthosite or mantled by plagioclase in olivine rim embayments (similar to Bell and Claydon [1992] for the Skye layered intrusion) (e.g. see Figures 4e and h in O'Driscoll et al., 2010). Similar textural associations are observed in other layered intrusions (see Lenaz et al., 2011). At the Unit 7-8 boundary (O'Driscoll et al. 2009b), spinel shows two trends, with large Al/(Al+Cr) and Fe^{3+} variations (Figure

8a). At the Unit 11-12 boundary (O'Driscoll et al., 2010), spinels show limited Fe^{3+}-enrichment, but the strongest Al/(Al+Cr) variation.

In Unit 9, the spinel grains are disseminated throughout the cumulates (i.e. mostly peridotite, troctolite and rare anorthosite). Spinel grains from the Unit 9 matrix (i.e. not fully included in olivine, plagioclase or clinopyroxene) analysed by Holness et al. (2007) and Leuthold et al. (2014a) generally have a higher Cr# (0.53 to 0.03) than grains crystallized along the B62/2 picrite QFM liquid line of descent (0.38 to 0.06) (Figure 8). The Cr-spinel Al/(Cr+Al) ratio shows limited variation and Fe^{3+} strongly increases from anorthosite to peridotite, troctolite, gabbro and poikilitic gabbro. Spinel grains in most poikilitic gabbros and one troctolite sample have low Mg#, TiO_2 and Cr# contents (Figures 6, 7, 8). In peridotite, and rarely troctolite, Al-poor spinel occurs as inclusion in olivine or in olivine-hosted recrystallized melt inclusions, in association with hornblende, orthopyroxene, and aspidolite (Leuthold et al., 2014a). Similar recrystallized melt inclusions have been documented in layered intrusions and oceanic lower crust gabbro (e.g. Irvine, 1975; Arai et al., 1997; Spandler et al., 2005; Renna and Tribuzio, 2011). Spinel itself hosts recrystallized melt inclusions consisting of olivine, plagioclase, apatite and Ti-spinel. The Unit 9 spinel Cr# is distinctly higher (up to 0.53 in anorthosite and 0.51 in troctolite) then the Unit 7-8 and 11-12 boundary discussed above and may have a different petrogenesis, as follows.

Olivine:

The Unit 9 profile F olivine composition is Fo_{80-75} (Holness et al., 2007). In the profile M area, where reactive liquid flow processes have been characterized in detail (Leuthold et al., 2014a), the olivine composition varies from Fo_{85} in peridotite to Fo_{84-82} in troctolite, to Fo_{84-81} in gabbro and Fo_{82-79} in poikilitic gabbro.

Plagioclase:

The plagioclase anorthite content along profile F varies from An_{79} to An_{69} with normal zoning down to An_{65}. In the area studied by Leuthold et al. (2014a), the plagioclase anorthite content (An_{85-80}) shows very little variation. Along profile F (400m to the North), it is An_{79-69} and along profile G (300m further to the North, above a peridotite lens) (Holness et al., 2007) it is An_{90-80}. The Fe_2O_3 content is 0.60 wt% for peridotite, troctolite and gabbro and 0.68 wt% for poikilitic gabbro (Leuthold et al., 2014a).

Clinopyroxene:

In Rum Unit 9, the clinopyroxene composition varies widely (Leuthold et al., 2014a). Whereas Fe-Mg cations were locally re-equilibrated, Cr and Al still record the original clinopyroxene composition obtained during precipitation from the melt (Leuthold et al., 2014a). Clinopyroxene core concentrations of Cr and Al show strong variations throughout the cumulate pile, from peridotite (Mg# = 0.89-0.86, Cr_2O_3 = 1.2-1.1 wt%, Al_2O_3 = 3.3-3.2 wt%), to troctolite (Mg# = 0.87-0.85, Cr_2O_3 = 1.2-1 wt%, Al_2O_3 = 3.7-3.2 wt%) and gabbro (Mg# = 0.86-0.80, Cr_2O_3 = 1.0-0.2 wt%, Al_2O_3 = 3.5-2.4 wt%) consistent with Cr depletion during progressive crystallisation. Clinopyroxene rims show strong zoning in peridotite (Mg# = 0.87-0.86, Cr_2O_3 = 0.86-0.85 wt%, Al_2O_3 = 3.1-2.9 wt%) and troctolite (Mg# = 0.86-0.84, Cr_2O_3 = 1.0-0.5 wt%, Al_2O_3 = 3.2-2.7 wt%) and no distinct zoning in gabbro (Mg# = 0.85-0.80, Cr_2O_3 = 1.0-0.3 wt%, Al_2O_3 = 3.2-2.4 wt%). Zoning in poikilitic gabbro is strong and complex (Mg# varies from 0.85-0.82 in the core to 0.85-0.82 in the rim, Cr_2O_3 varies from

1.2 to 0.1 wt%, Al_2O_3 varies from 3.7 to 2.3 wt%, TiO_2 varies from 0.58 to 1.2 wt%) (see Leuthold et al., 2014 for details). Clinopyroxene analyses from a single rock sampled 6m below the top of profile F show low Mg# (0.86-0.81), Cr_2O_3 (0.57-0.14 wt%) and Al_2O_3 (3.2-2.2 wt%) concentrations (unpublished data).

Discussion:

Controls on the stability and chemistry of spinel:

Because of the distinctive chemical variation in spinels from Rum and other layered intrusions and the widespread usage of spinel as a petrogenetic indicator, it is informative to use our experiments, in conjunction with published experiments (Murck and Campbell, 1986; Roeder and Reynolds, 1991), to elucidate the important controls on spinel composition. The key parameters responsible for Cr-spinel chemistry are shown schematically in Figure 10.

Liquid composition:

In order to saturate in Cr-spinel, the parental liquid must be TiO_2-poor (<2.8 wt%), have a low FeO/MgO ratio (<2.0) and contain more than 200 μg/g (ppm) Cr (Thy, 1983). Unlike the other major elements in the spinel structure, Cr acts as a trace element in the parental liquid (Ridley, 1977). Allan et al. (1988) proposed that the Cr content of spinels within a given magma has little relationship to host-liquid Cr content but instead is indirectly controlled by the host magma Al, Fe^{2+}, and Mg contents. Our Cr-rich (picrite) and Cr-poor (basalt) experiments and MELTS calculations refine that proposal: MELTS calculations show that an increase in the starting liquid Cr_2O_3 results in saturation of Cr-enriched spinel at a higher temperature, but its composition at similar temperatures does not change (an addition of 0.2 wt% Cr_2O_3 to the starting picrite liquid increases Cr-spinel saturation by 150°C and Cr# from 0.41 to 0.60). Hill and Roeder (1974) also showed that the spinel liquidus is shifted to higher temperature when Cr_2O_3 is added to the starting material. The spinel saturation in Cr-poor basalt experiments is delayed in comparison to Cr-rich picrite experiments and the basalt liquid line of descent lacks Al-rich spinel. According to Kamenetsky et al. (2001), the spinel Mg# at magmatic conditions is directly linked to the parental melt Mg# and Al_2O_3 content. Murck and Campbell (1986) showed that upon cooling from 1450 to 1150°C, spinel becomes progressively less Cr-rich. This trend is consistent with our experiments, and points to the high-temperature Cr depletion of Cr_2O_3-doped melts close to their liquidus (Figure 8c).

Liquid composition directly affects mineral saturation temperatures. Our results confirm the observations by Roeder and Reynolds (1991; and references therein) that plagioclase and clinopyroxene stability plays a major role in determining spinel composition, by controlling liquid Al_2O_3 and Cr_2O_3 contents. In picrite experiments, the crystallization of abundant (up to 30 vol%, Table 2) clinopyroxene, accommodating significant amounts of Cr, effectively depletes the liquid in Cr_2O_3, thus driving the spinel chemistry towards Cr-poor composition. The Cr-spinel crystals with the lowest Al/(Cr+Al) ratio and Fe^{3+} concentration crystallize from plagioclase-rich, clinopyroxene-depleted picrite-troctolite hybrid melt (Figure 8c). A similar Fe^{3+}-enrichment trend would be expected in gabbro hybrid experiments, however the selected gabbro FeO_{tot} is rather low (5.49 wt% FeO_{tot}). Hybridization with low-Fe gabbro decreases the liquid Fe content and spinel remains low in Fe over a large temperature range (Figures 6, 8c). At high temperature, in low-Fe picrite-gabbro and gabbro experiments, olivine also has a high forsterite content at high temperature. We have run additional MELTS calculations using a picrite doped with 50% plagioclase as starting composition. The chemistry of Cr-spinel is slightly more Cr-rich along

fractional liquid line of descent and slightly less Cr-rich along equilibrium liquid line of descent than for picrite-only calculations. The plagioclase abundance and increased stability balance the melt enrichment in Al_2O_3, resulting in a minor effect on spinel chemistry.

Temperature:

The Fe-Mg exchange between spinel and olivine is temperature-sensitive, with Mg preferentially partitioning into olivine with decreasing temperature (Roeder et al., 1979) and has been used as thermometer (e.g. Irvine, 1965; Roeder et al., 1979; Engi, 1983). Diffusion (discussed below) in the Fe-Mg sites continues at sub-solidus conditions (O'Driscoll et al., 2010). Wilson (1982) concluded that geothermometers based on chromite-silicate equilibria are probably not applicable to slowly-cooled layered intrusions, but information on thermal histories may be gleaned from diffusion profiles.

Pressure and water:

Spinel is stable from mantle conditions to atmospheric pressure. Dick and Bullen (1984) proposed that Cr solubility in the melt is increased at high pressure. Fisk and Bence (1980) and Roeder and Reynolds (1991) proposed Cr# decreases at higher pressure (at conditions above the plagioclase saturation temperature), accompanied by an increase in Mg# and decrease in Fe^{3+}. Feig et al. (2006) performed oxidized experiments over a wide range of P-T-H_2O conditions on tholeiitic basalts inferring that spinel Cr# decreases as pressure increases from 100 MPa to 200 MPa, followed by a constant value up to 500 MPa. In contrast, Sisson and Grove (1993a, 1993b) showed that in calc-alkaline, high-alumina basalt experiments at NNO, water-saturated conditions, 1100°C and 100 MPa, spinel (co-saturated with olivine) has a lower Cr# than at 1050°C and 200 MPa.

Pressure or water variations have limited effect on spinel composition, but do significantly modify the stability and composition of coexisting plagioclase and clinopyroxene. At higher pressure and/or water content, plagioclase saturation is delayed and clinopyroxene stability increases, resulting in an increased spinel Al/(Cr+Al) ratio. In Feig et al's (2006) experiments, spinel stability increases at high water content (>3 wt%), whereas plagioclase stability is decreased. At such conditions, clinopyroxene saturates prior to plagioclase and coexists with Cr-spinel. In this particular case, the water content was directly and positively linked with oxygen fugacity and thus, spinel in hydrated melts resulted in higher Fe^{3+}, due to H_2-loss. At similar water activities and temperature, spinel in high-pressure experiments is slightly more Fe^{3+}-rich and Cr-poor, because spinel saturation temperature is increased. Thus, low-pressure spinels have the capacity to attain the highest Cr# for a given bulk liquid composition. The Fe# and TiO_2 are only marginally affected by pressure and H_2O variations at a given fO_2.

Oxygen fugacity:

Fe^{3+} stabilizes spinel, hence increasing fO_2 promotes precipitation of abundant Fe^{3+}-rich spinel from basaltic liquids (Hill and Roeder, 1974; Ridley, 1977; Sharpe and Irvine, 1983; Murck and Campbell, 1986). Our experiments produce abundant (~1 vol%) Fe^{3+}-rich spinel at QFM+1.8. In the picrite, picrite-gabbro and gabbro experiments at and above QFM, spinel co-exists with olivine, plagioclase and clinopyroxene over ~40°C (Figure 4), until the liquid Cr-content is depleted to such an extent that chromite is no longer stable (Irvine 1967). This

contrasts with the generally accepted idea that spinel + melt would react to clinopyroxene or to olivine + anorthite via peritectic reactions (Irvine, 1967; Hill and Roeder, 1974; Roeder, 1994) at low pressure (< ~0.5 GPa, Grove et al., 1992). This principle is adapted from the haplobasaltic, Cr- and Fe-free forsterite-anorthite-diopside system where the non-ternary, spinel phase ($MgAl_2O_4$) field is terminated at a divergent peritectic point followed down-temperature by the forsterite-anorthite cotectic (Morse et al., 1980; Soulard et al., 1994). This system cannot, however, be used to to infer phase equilibria between Cr-Al-Fe-Mg spinels and silicate phases where complex solid solutions exist and the degree of freedom is increased due to at least 5 additional relevant components (Fe, O, Cr, Ti and Na) allowing for large stability fields wherein spinel coexists with three or more silicate mineral phases plus melt. Hill and Roeder (1974) showed a gap in spinel crystallization under reduced conditions, where Cr-spinel is replaced by clinopyroxene in a peritectic reaction and only reoccurs at low temperature as Ti-magnetite (or ulvospinel). Our experiments confirm Fe^{3+}-poor spinel occurs only in trace amounts at QFM-2.2 and temperatures in excess of 1180°C; it is absent in lower temperature runs.

Differentiation:

The 11JL33 basalt represents a fractionated liquid from a parental Rum B62/2 picrite. Crystal chemistry in both liquid lines of descent follows a similar evolution, but basalt experiments lack the most primitive crystals found in the picrate experiments (Figures 6, 8c). MELTS calculations show that spinels crystallized via equilibrium or fractional crystallization along the QFM liquid line of descent differ little in their composition (Figure 8b). Spinels obtained in the QFM cooling-rate experiments show very limited Cr-enrichment compared to isothermal experiments. Conversely, MELTS fractional crystallization calculations performed under reducing conditions produce more Cr-rich spinel than equilibrium crystallization (Figure 8b). Leaving the oxygen fugacity free in MELTS calculations produces spinel with even higher Cr#, especially for initially reduced conditions.

In plagioclase-saturated experiments, spinels have a slightly lower Al/(Cr+Al) ratio and lower Fe^{3+} in cooling-rate experiments (simulating inefficient fractional crystallization) than in isothermal experiments (true equilibrium crystallization). The glass composition is also slightly depleted in Al_2O_3 in cooling-rate experiments. The estimated plagioclase modes are not systematically higher in cooling-rate experiments, but the anorthite content is. Thus, plagioclase crystallization directly influences spinel chemistry.

Irvine (1975) proposed that increased melt polymerization (NBO/T; e.g. by increased silica content) would decrease the number of octahedral sites in the melt. As Cr cations have a strong preference for octahedral sites (Burns, 1975), increased polymerization would significantly reduce Cr-spinel solubility in the melt, promoting early Cr-spinel precipitation. According to Thy et al. (1983), local depletion in melt Cr content is due to crystallization of Cr-spinel, with large spinel/melt partition coefficient for Cr (Hill and Roeder 1974). Such small-scale fractionation may be responsible for grain-to-grain variation in Cr# with relatively constant A1/Fe^{3+} and a lack of correlation with Mg#. Our observations infer that the small proportion of Cr-spinel equilibrium crystallization at high temperature has little effect on the spinel and liquid Cr-contents. In contrast, the crystallization of abundant clinopyroxene effectively depletes both the liquid and coexisting spinel in Cr over a small temperature range.

Re-equilibration:

Irvine (1980) pointed out that even cumulus grains whose textures do not appear to have been modified may

have had their composition changed extensively by reactive liquid flow processes (i.e. postcumulus metasomatism, as defined by Irvine, 1982). In spinels Fe^{2+} - Mg; Cr – Al; Fe^{3+} - Cr, Al; Fe, Ti – Cr, Al cation substitutions take place (Ridley, 1977). In the $FeAl_2O_4$-$MgAl_2O_4$ system, intra-spinel and spinel-melt and spinel-olivine Fe^{2+}-Mg diffusion are very fast, whereas spinel-melt Al, Cr, Fe^{3+} and Ti diffusion rates are slow (Wilson, 1982; Ozawa, 1984; Scowen et al., 1991; Allan, 1994; Roeder et al., 2001; Suzuki et al., 2008). Consequently sub-solidus reactions only allow Fe-Mg exchanges (O'Driscoll et al., 2010). At near- and sub-solidus conditions, spinel Mg# is controlled by the rate of cooling and re-equilibration with silicates (Kamenetsky et al., 2001). Hoshide and Obata (2014) showed Cr-spinel Fe^{3+}-enrichment, with very limited Cr^{3+}-enrichment, when re-equilibrated with evolved interstitial melt. Significant diffusion can occur through and within olivine and modify spinel inclusion compositions (Scowen et al., 1991; Hoshide and Obata, 2014), which should not therefore be used as indicators of original liquidus compositions. Diffusion through plagioclase is slower and the chemistry of spinel inclusions is less modified as a consequence (Hoshide and Obata, 2014).

Bell and Claydon (1992) proposed that Al-rich Cr-spinel reacts with Ca-rich melt to produce plagioclase, olivine and Cr-rich spinel, accompanied by a decrease in Mg# and increase in TiO_2. This peritectic reaction explains the increased amounts of intercumulus plagioclase and the small amounts of intercumulus olivine associated with the more chromian spinel present in layered intrusions (e.g. O'Driscoll et al., 2009b). More Ti-rich, Al-poor Rum spinel equilibrated over a long period of time at a low temperature with intercumulus melt (O'Driscoll et al., 2010; Lenaz et al., 2011). O'Driscoll et al. (2010) indicate the importance of the modal proportion of spinel in buffering the reaction: the more abundant it is, the less the re-equilibration.

Petrogenesis of Cr-spinel in the Rum Eastern Layered Intrusion:

Unit 7-8 and 11-12 boundary Al-spinel seams:

Rum spinel petrogenesis has long been discussed. Henderson and Suddaby (1971), Henderson (1975), Putnis and Price (1979) and Henderson and Wood (1981) have shown that seam spinels are much more Al-rich and Cr-poor and have a lower Fe# than spinels in the nearby plagioclase-rich rock and overlying peridotite. Chromite Al-enrichment can result from the reaction with olivine and either plagioclase or from a melt rich in plagioclase component, a reaction known as the 'Rum trend' (Barnes and Roeder, 2001 after Henderson, 1975). Fe^{3+}-enrichment, on the other hand, is interpreted as progressive crystallization or reaction with evolved interstitial liquid (Henderson, 1975; O'Driscoll et al., 2010). Young (1984) suggested that in Unit 7 evolved, interstitial basaltic liquid migrated upward from the troctolite and anorthosite crystal mush, blended with newly injected picrite and created a hybrid magma saturated with Cr-spinel (i.e. the model of Irvine, 1977). For Dunham and Wadsworth (1978), the occurrence of the Unit 11-12 chromitite bands within a zone whose mineralogy shows rapid changes from Fe-Na to Mg-Ca-rich minerals (i.e. a reverse of the normal magmatic trend) reflects the influx of new Mg-rich magma into the system. In particular, Dunham and Wadsworth (1978) suggest that the Mg- and Al-rich spinel had crystallized directly from the picrite, without subsequent reaction with the crystal mush or interstitial liquid. O'Driscoll et al. (2009b, 2010) showed that the chemistry of Cr-spinel at the boundary between Units 7 and 8 evolved towards a low Al concentration prior to a progressive Fe^{3+} enrichment at constant Cr# (Figure 8). They proposed a model whereby Cr-spinel crystallized in-situ, from a hybrid melt produced by assimilation of troctolite cumulate into infiltrating reactive picritic liquid, one of the processes simulated in our experimental study.

Following Irvine (1977), Roeder and Reynolds (1991) proposed that mixing of a hot, plagioclase-undersaturated, primitive magma, with a plagioclase-enriched magma could produce hybrid melts that crystallize chromite with low and highly variable Cr#. Magma mixing and dissolution of plagioclase could also have been responsible for the so-called alumina Rum trend described above. Following these ideas, O'Driscoll et al. (2009b, 2010) proposed a model whereby abundant picritic liquid (i.e. a mafic olivine-saturated liquid) percolated and assimilated troctolite cumulate to produce a plagioclase-saturated melt. The hydrid melt then crystallized Cr-spinel seams (~2mm thick) and anorthosite (~10-70cm thick). Our experiments show 50%-50% mixing of picrite and troctolite liquids produces a hybrid melt that crystallizes Al-rich spinel and olivine at liquidus temperature, thereafter fractionating abundant plagioclase ($\sim An_{86}$) from 1240°C and saturating in clinopyroxene at 1160°C. The Al/(Cr+Al) ratio of high-temperature Al-spinel decreases dramatically upon cooling, reaching the highest measured Cr# of 0.54 at 1180°C at QFM-1.2, before it quickly evolves towards Fe^{3+}-rich composition (Figure 8c). The Units 7-8 and 11-12 Al-rich spinel seams (Al/[Cr+Al] as high as 0.70) are therefore consistent with crystallization from picrite-troctolite hybrid liquid, as suggested by O'Driscoll et al. (2009b, 2010), at a temperature close to 1210°C and QFM condition. This temperature is higher than that determined for natural grains utilising the olivine-spinel exchange thermometer of Ballhaus et al. (1991) and Princivalle et al. (1999) (see O'Driscoll et al., 2009b and Lenaz et al., 2011), a fact we attribute to re-equilibration during cooling.

In our experiments, the Al- and Cr-spinel modal proportions are low (typically 0.1-0.2 vol%) and the crystallization of a 2mm thick seam with 30 vol% spinel requires effective sorting and settling of denser spinel from a 30-60 cm thick magma layer, in agreement with field observations. Spinel extraction from a basaltic liquid appears to be very efficient (Manoochehri and Schmidt, 2014). At ~1230 to ~1180°C, the liquid fraction amounts to 60-30 vol% in picrite-troctolite hybrid magma, allowing dense crystals to settle out as long as they are not part of a touching framework. This model could explain the formation of the main spinel seam, at the interface between peridotite (picrite) and anorthosite/troctolite.

Subsidiary spinel seams are sandwiched between overlying peridotite and troctolite. Spinel often occurs in indentations and embayment structures in olivine oikocrysts (see Figure 3 in O'Driscoll et al., 2009b). In our reaction experiments, we have tested the effect of chemical disequilibrium between picrite and troctolite melt at constant temperature, pressure and oxygen fugacity. Through picrite liquid hybridization with troctolite partial melt, the glass and the spinel Al and Cr compositions vary considerably and the spinel modal abundance increases markedly (up to 3.5vol%; Figure 9). Despite the low oxygen fugacity, the spinel proportion is the highest we have measured. These observations corroborate the model of spinel seam formation during picrite-troctolite melt hybridization. Subsequent plagioclase fractionation increases the spinel Cr#. It is curious to note abundant Cr-spinel crystallized in the picrite-troctolite reaction zone, where plagioclase is absent. We hypothesise that picritic liquid percolated into the troctolite crystal mush and dissolved plagioclase, which is unstable at 1250°C. The melt Al-content increased, stabilizing spinel that crystallized between relict olivine grains. As the picrite Cr-content is high and spinel is the only phase incorporating Cr into its structure, Al- and Cr-rich spinel crystallizes. The Cr-rich picrite and Al-rich troctolite melt ratio is crucial here. Based on the observation that the spinel composition in reaction experiments spans the range of spinel crystallized from equilibrium experiments, we suggest that spinel with higher Cr# crystallized at lower temperature (upon cooling or during reaction at lower temperature). However, evidence for reaction seems to disappear over prolonged

reaction time. Additionally, spinel is modally more abundant on the troctolite side of the reaction rim, at ca. 100 µm from the picrite contact. This observation supports in-situ spinel subsidiary seams crystallization as opposed to gravitational settling of dense spinel. Upon cooling, the hybrid melt will fractionate abundant plagioclase, forming the anorthosite.

Unit 9 Cr-spinel:

We established earlier that distinct physico-chemical parameters can increase the spinel Cr# of a single magma, approaching those found in Rum Unit 9 (Figure 10): (1) Low water content increases plagioclase stability and Al depletion; (2) low pressure reduces clinopyroxene stability and Cr extraction and also raises the melt and spinel Cr-content, at sub-liquidus condition; (3) spinel Cr_2O_3 concentrations are higher under low fO_2 conditions, but its modal abundance is strongly reduced. The corroded texture observed at intermediate temperature (1180°C, QFM-2.2) indicates a peritectic reaction with the liquid and clinopyroxene. Crystallization of abundant chromite cannot be explained by low fO_2 conditions alone, unless crystallized over a small temperature interval from a very large magma body or from a clinopyroxene-depleted magma; (4) fractional crystallization has a strong effect on the spinel Cr-enrichment at low fO_2, but spinel becomes unstable at low temperature under reduced conditions; and (5) spinel Cr# increases through re-equilibration with plagioclase + melt or clinopyroxene + melt (Wilson, 1982; Bédard and Hébert, 1998).

High Cr# and Ti and low Mg# and Al spinel, with a composition very close to the Unit 9 Cr-rich spinel (Figures 7, 8), crystallize from picrite-troctolite hybrid melt at QFM-1.2, 1180°C. Clinopyroxene saturation is delayed in picrite-troctolite hybrid experiments, permitting the crystallization of high Cr# spinel even under reduced conditions. Spinels obtained by MELTS fractionation calculations and from the cooling-rate experiments have a higher Cr# than those from MELTS equilibrium calculations and from isothermal experiments respectively. Olivine and plagioclase fractionation could further drive the spinel chemistry towards the Unit 9 chromite composition. Also, higher Cr# spinel crystallizes from MELTS calculations where the fO_2 is allowed to vary (especially for initially reduced conditions). Those two processes were not investigated during our experiments and may account for the minor differences between experimental and natural crystals. Fe-Mg diffusion occurs down to sub-solidus conditions (O'Driscoll et al., 2010) and may have lowered the Unit 9 spinel Mg# (Roeder et al., 1979; Scowen et al., 1991; Kamenetsky et al., 2001). We propose the Unit 9 Cr-spinels fractionated over a limited temperature range (ca.1180°C), from a reduced picrite-troctolite hybrid melt fractionating olivine + plagioclase. These spinels subsequently experienced sub-solidus re-equilibration with olivine.

Unit 9 and 7-8 boundary Fe^{3+}-rich spinel:

Spinel crystals in picrite and basalt cooling-rate experiments at QFM, ~1125°C and QFM+1.8 ~1180°C have a similar composition to the troctolite, gabbro and poikilitic gabbro Fe^{3+}- and Ti-rich crystals suggestive of crystallization at such conditions. Alternatively, equilibration of isolated Cr-spinel with evolved interstitial melt would likewise increase the spinel Fe^{3+} content observed in those lithologies (Henderson, 1975; Hoshide and Obata, 2014). O'Driscoll et al. (2010) inferred that the extent of spinel textural and chemical re-equilibration is inversely proportional to the spinel modal abundance. Thus, re-equilibration of low modal proportions of Cr-spinel with trapped melt (crystallizing abundant Fe-poor plagioclase; Lenaz et al., 2011) could induce strong

Fe^{3+}-enrichment. Fe^{3+}-rich spinel indeed occurs in the least compacted cumulates (i.e. gabbro and poikilitic gabbro) (Leuthold et al., 2014a). Ridley (1977) suggested an extensive solid solution between Cr+Al and Ti+Fe spinels. Rum Cr-spinel grains show post-cumulus Cr- and Al-increase and Fe- and Ti-decrease towards the contact with ilmenite crystals (not shown), possibly produced by spinel oxidation down to ~600°C (Putnis and Price, 1979; O'Driscoll et al., 2010). Finally, Bell and Claydon (1992) proposed that the spinel grains may have been modified by postcumulus peritectic reaction of Al-rich spinel with melt producing low Mg# and Cr-, Fe^{2+}-, Fe^{3+}-, Ti-rich spinel + plagioclase + olivine. This trend is similar to that in our picrite experiments. Ultimately, in order to explain the Unit 9 titanomagnetite petrogenesis it is difficult to distinguish between (1) crystallization from a differentiated liquid at QFM or more oxidized conditions, or (2) re-equilibration with a differentiated melt. Both processes overlap when interstitial melt is not efficiently extracted.

M9 picrite accumulated spinel:

Spinel in the olivine- and spinel-phyric picritic dyke M9 (Upton et al., 2002; O'Driscoll et al., 2010) have low Ti, Cr# and $Fe^{2+}/(Mg+Fe^{2+})$ in comparison to the Unit 9 grains (Figure 7). Upton et al. (2002) suggested the M9 olivine and spinel primocrysts formed at high pressure in a near-Moho reservoir from a high MgO melt (~20wt%) (Upton et al., 2002), prior to remobilisation by picritic liquid (~13wt% MgO) and emplacement into the Rum Eastern Layered Intrusion. MELTS calculations of picrite at high pressure (0.3 GPa) predict that spinel crystallized at sub-liquidus temperature from a Cr-rich liquid, or under reduced conditions, has a high Cr# similar to natural grains (Figure 8). The melt Cr_2O_3 content determines the Cr# of the first spinel to saturate, directly influencing the saturation temperature. Looking at Figures 8b and c, spinel Cr# is high at very high temperature, prior to Al-increase. Thus, M9 spinel primocrysts may have crystallized at very high temperature and lower crustal pressure from a more mafic melt than the Unit 9 crystals (i.e. less TiO_2 and FeO and more MgO and Cr_2O_3; Fisk and Bence, 1980) prior to emplacement. It is probable that a few Unit 9 spinels were inherited from an M9-type dyke, and then re-equilibrated during hybridization with partially molten mafic crystal mushes.

Petrogenesis of the Rum Unit 9 cumulates:

Using our picrite and basalt experiments together with the large dataset of natural crystals compositions (Holness et al., 2007; Leuthold et al., 2014a), we attempt to determine the physico-chemical conditions for the formation of the Rum Unit 9 cumulates. In the Appendix table 3, we present correspondences based on the Figure 6. We will first compare the natural grains with the Rum picrite and basalt equilibrium liquid lines of descent. Leuthold et al. (2014a) proposed the phase abundance, saturation temperature and chemistry were shifted from the equilibrium liquid line of descent though *reactive liquid flow* (Figure 1). We then test the hypothesis that the Unit 9 cumulates were modified by gabbro and/or troctolite assimilation. It is believed that cumulates in the profile F area (see Appendix figure 1), where the discordant peridotite sill is absent, were not modified by late-stage crystal-melt reactions, thus still showing the original composition.

Olivine

Olivines in profile F are distinctly more fayalitic (Fo_{82-74}) than along other Unit 9 profiles E, G, H and I (Fo_{87-80}) sampled by Holness et al. (2007). Although we cannot exclude the possibility that the Rum olivine

composition was not fully re-equilibrated, the olivine compositions obtained in the picrite (for all fO_2 conditions), picrite-gabbro and picrite-troctolite experiments overlap with the range of Unit 9 crystals overlying peridotite sills (Figure 6). Olivine in basalt experiments is more Fe-rich, consistent with the down-temperature extension of the picrite experiments. Thus profile F olivines are consistent with low temperature picrite and/or hot basalt parental liquids.

Plagioclase

Plagioclase in Rum Unit 9 shows lateral chemical variability, ranging from An_{85-80} in the area studied by Leuthold et al. (2014a) to An_{79-69} 400m to the North, along profile F of Holness et al. (2007) and An_{90-80} along profile G 300m further North. While the chemistry of profile F crystals is well reproduced by picrite experiments and corresponds to the range from the point of plagioclase saturation to the solidus, the high anorthite content of Leuthold et al. (2014a) and profile G (Holness et al., 2007) can only be reproduced by hybrid experiments. Alternatively, crystallization from a water-bearing magma would lower the plagioclase liquidus temperature and crystallise plagioclases that are higher in An content (Kuritani, 1998). MELTS calculations at the maximal estimated crystallization pressure of 50 MPa (Holness, 1999) reveal little effect on the anorthite composition compared to 0.001 MPa. Along a fractional crystallization liquid line of descent, the anorthite content would become even lower (e.g. Toplis and Carroll, 1996). Anhedral cores, also described by Young (1984) and O'Driscoll et al. (2009b) in the Unit 7, are An_{68-58}, similarly to the 11JL33 basaltic dyke experiments. Anhedral sodic cores certainly crystallized from a basaltic parental magma or from a fractionating dry picritic liquid.

The Unit 9 plagioclase Fe_2O_3 content varies from 0.4 to 0.8 wt%, with no distinction between core, rim and anhedral core (profiles F and G in Holness et al., 2007; Leuthold et al., 2014a). In picrite and basalt experiments, plagioclase Fe_2O_3 increases from ~0.6 to ~1.8 wt% at QFM and is <0.7 wt% under more reduced conditions. Plagioclase crystallized from hybrid experiments have Fe_2O_3 concentration ranging from 0 to 1.5wt%. Thus, unmodified profile F natural plagioclase grains are consistent with crystallization from a hot (~1140°C), wet, reduced (~QFM-1.2, possibly up to QFM) basalt. Conversely, the more An-rich crystals above peridotite sills crystallized either from a hot water-bearing reduced picritic melt or a hybrid melt.

Clinopyroxene

The Mg# of cumulate crystals (0.89-0.80 in the profile M area, ~0.86-0.79 along profile F) is higher than those in experiments, except for the high-temperature, reduced picrite, picrite-gabbro and gabbro experiments. According to Leuthold et al. (2014a), divalent cations were frequently partly re-equilibrated (at least within the individual grains) but trivalent cations were unmodified The Cr_2O_3 concentration of the experimental clinopyroxene overlaps with the clinopyroxene core composition from all lithologies, except for the Cr_2O_3-poor basalt experiments. Profile F clinopyroxene has low Cr-contents identical to basalt and low-temperature picrite experiments. Only clinopyroxene crystallized from reduced experiments at high temperature (picrite, basalt, picrite-gabbro, gabbro and picrite-troctolite) have low Al_2O_3, close to natural Unit 9 grains in the profile M area.

Synthesis

Comparing olivine, plagioclase and clinopyroxene to experimental crystals shows the Unit 9 profile F gabbro crystallized from a hot (~1140°C), wet, reduced basalt at QFM-1.2, possibly up to QFM). Clinopyroxene

cores, plagioclase and olivine in the profiles M, G, H, E area crystallized from a hot (~1180°C), reduced (~QFM-1.2) picrite. Lateral variations may be explained by local accumulation of high temperature crystals and the segregation of interstitial melt that will fractionate down-temperature. Also gravity currents (Emeleus et al., 1996; Tepley and Davidson, 2003; O'Driscoll et al., 2007) may transport and juxtapose grains crystallized at different conditions.

Picrite or basalt liquid lines of descent fail to reproduce the profile M area crystal cumulates. The most likely parental melts are picrite-gabbro, gabbro or picrite-troctolite crystallizing at ~1170°C and reduced conditions. Subsequent to hot reactive picrite intrusion, the chemistry and composition of the overlying cumulative rocks was modified during *reactive liquid flow*. Where low-degree gabbro partial melting was achieved (a few decametres from the sill, according to Leuthold et al., 2014), clinopyroxene crystallized around pre-existing, partially molten crystals from a reduced gabbro melt, or reduced picrite-gabbro hybrid melt where porosity was sufficient for both melts to mix, forming complex poikilitic gabbro. Closer to the peridotite sill, the high-An, low Fe_2O_3 troctolite plagioclase indicates crystallization from a reduced hybrid picrite-troctolite melt. This is consistent with the low abundance of clinopyroxene, depleted by troctolite assimilation and the chemical constraints from spinel. Our experiments highlight an increased melting proportion of plagioclase versus clinopyroxene towards the peridotite sill. Based on successive crystallization-dissolution stages in clinopyroxene, Leuthold et al. (2014a) have demonstrated consecutive partial melting episodes. This suggests most clinopyroxene close to the hot intrusive sill was molten and expelled, leaving a troctolite restite that was intruded and partially melted next to a second hot picrite intrusion. Spinel, An-rich plagioclase and sparse clinopyroxene crystallized from this later, hot, reduced hybrid picrite-troctolite melt at ~1190-1160°C. Exact temperature estimates may vary slightly vary (not more than ~20°C), when considering different picrite-gabbro and picrite-troctolite proportions.

Conclusions:

We have determined the Rum parental magma liquid line of descent over a wide range of oxygen fugacity, from liquidus to solidus conditions. The plagioclase saturation temperature is only slightly higher than that of clinopyroxene. We observe excellent agreement with MELTS calculations (Ghiorso and Sack, 1995; Asimow and Ghiorso, 1998) in terms of crystal saturation temperatures and modal abundances increasing confidence in this algorithm for understanding Rum petrogenesis. The temperatures and modes used in the reactive liquid flow model by Leuthold et al. (2014a) are thus corroborated. Using the plagioclase and clinopyroxene chemistry in Unit 9 and in experiments, we propose that the Rum parental magma was slightly reduced (around QFM-1.2).

We have studied experimentally the effect of mafic cumulate (gabbro and troctolite) melting by cogenetic picrite liquid and melts hybridization. The liquidus and solidus temperatures are shifted from the picrite liquid line of descent in hybrid experiments, in accordance with the cumulate equilibrium temperature. Mineral modes are strongly modified. The plagioclase fraction, in particular, is increased significantly. Assimilation of mafic crystals by mafic melt has a minor, but distinct, effect on the chemistry of the new crystal generation. High temperature troctolite assimilation decreases spinel Fe#, Cr# and TiO_2 concentration. This is best explained by olivine and plagioclase dissolution, releasing MgO and Al_2O_3 to the hybrid melt. Down-temperature, abundant plagioclase crystallization strongly depletes the residual melt in Al_2O_3, driving the spinel towards low Al/(Cr+Al). Clinopyroxene removes Cr_2O_3 from the melt, but its stability is reduced in such compositions,

favouring crystallization of high Cr# spinel. Chromites from Rum Unit 9 are best explained by troctolite assimilation into invading reactive picrite and crystallization from a hybrid melt. Clinopyroxene and plagioclase compositions cannot be explained simply by crystallization from pure picrite or basalt liquid and also require hybridization with various proportions of gabbro and/or troctolite. Our observations confirm the model of Cr- and Al-spinel precipitation from a hybrid picrite-troctolite melt, proposed by O'Driscoll et al. (2009b, 2010) and Leuthold et al. (2014a). Our combination of natural observations and experiments allowed us to determine the crystallization temperature and parental melt chemistry of the complex Rum Eastern Layered Intrusion cumulates.

Acknowledgements:

Special thanks are due to Stuart Kearns and Ben Buse for technical assistance with the FEG-EMPA. Many thanks to Peter Ulmer for his constructive comments and help writing this manuscript. We acknowledge Keith Putirka, an anonymous reviewer and editor Tim Grove whose comments and remarks have helped to improve this paper. We thank Scottish Natural Heritage for granting permission to collect in the Rum Site of Special Scientific Interest. We acknowledge Brian Upton and Janet McClurg for lending us the Rum B62/2 picritic dyke powder. This study was supported by the Swiss National Science Foundation (SNSF) prospective researcher grant (PBLAP2- 134399/1) and Advanced Researcher grant (PA00P2_145348/1 and PA00P2_145348/3) to Julien Leuthold and ERC Advanced Grant CRITMAG to Jon Blundy.

References:

Allan JF, Sack RO, Batiza R (1988) Cr-rich spinels as petrogenetic indicators: MORB-type lavas from the Lamont seamont chain, eastern Pacific. Am Mineral 73: 741-753

Arai S, Matsukage K, Isode E, Vysotskiy S (1997) Concentration of incompatible elements in oceanic mantle: Effect of melt/wall interaction in stagnant or failed melt conduits within peridotite. Geochim Cosmochim Ac 61(3): 671-675

Asimow PD, Ghiorso MS (1998) Algortithmic modifications extending MELTS to calculate subsolidus phase relations. Am Mineral 83: 1127-1132

Ballhaus C, Berry RF, Green DH (1991) High pressure experimental calibration of the olivine-orthopyroxene-spinel oxygen geobarometer: implications for the oxidation state of the upper mantle. Contrib Mineral Petrol 107: 27–40

Barnes SJ, Roeder PL (2001) The range of spinel compositions in the terrestrial mafic and ultramafic rocks. J Petrol 42(12): 2279-2302.

Bédard J and Hébert R (1998) Formation of chromitites by assimilation of crustal pyroxenites and gabbros into peridotitic intrusions: North Arm Mountain massif, Bay of Islands ophiolite, Newfoundland, Canada. J Geophys Res 103(B3): 5165-5184

Bédard JH, Sparks RSJ, Renner R, Cheadle MJ, Hallworth MA (1988) Peridotite sills and metasomatic gabbros in the Eastern Layered Series of the Rhum complex. J Geol Soc London 145: 207-224

Bell BR, Claydon RV (1992) The cumulus and post-cumulus evolution of chrome-spinels in ultrabasic layered intrusions: Evidence from the Cuillin Igneous Complex, Isle of Skye, Scotland. Contrib Mineral Petrol 112: 242-253

Bell BR, Williamson IT (2002) Tertiary igneous activity. In: Trewin NH (ed) The geology of Scotland, 4th edn. Geol Soc London, London, pp 371–408

Brown GM (1956) The layered ultrabasic rocks of Rhum, Inner Hebrides. Philos T Roy Soc B 240: 1-68

Burns RG (1975) Crystal field effects in chromium and its partitioning in the mantle. Geochem Cosmochim Ac 39: 857-864

Cameron EN, Desborough GA (1969) Occurrence and characteristics of chromite deposits – eastern Bushveld Complex. Econ Geol Mon 4: 23-40

Campbell IH, Murck BW (1993) Petrology of the G and H chromitite zones in the Mountain View area of the Stillwater Complex, Montana. J Petrol 34(2): 291-316

Charlier B, Namur O, Toplis MJ, Schiano P, Cluzel N, Higgins MD, Vander Auwera J (2011) Large-scale silicate liquid immiscibility during differentiation of tholeiitic basalt to granite and the origin of the Daly gap. Geology 39: 907–910

Dick HJB, Bullen T (1984) Chromium spinel as a petrogenetic indicator in abyssal and alpine-type peridotites and spatially associated lavas Contrib Mineral Petrol 86: 54-76

Dungan MA, Davidson J (2004) Partial assimilative recycling of the mafic plutonic roots of arc volcanoes: An example from the Chilean Andes. Geology 32(9): 773-776

Dunham AC, Wadsworth WJ (1978) Cryptic variation in the Rhum layered intrusion. Mineral Mag 42: 347-356

Dunham AC, Wilkinson FCF (1985) Sulphide droplets and the Unit 11/12 chromite nand, Rhum: a mineralogical study. Geol Mag 122(5), 539-548

Emeleus CH, Cheadle MJ, Hunter RH, Upton BGJ, Wadsworth WJ (1996) The Rum Layered Suite. In: Cawthrorn RG (ed) Layered intrusions. Elsevier Science BV, pp 403-439

Emeleus CH (1997) Geology of Rum and the adjacent islands. Memoir of the British Geological Survey, Sheet 60 (Scotland)

Emeleus CH (2004) Rum solid geology map 1:20000. Scottish Natural Heritage

Emeleus CH, Gyopari MC (1992) British Tertiary Volcanic Province. Chapman & Hall, London

Engi M (1983) Equilibria involving Al-Cr spinel: Mg-Fe exchange with olivine. Experiments, thermodynamic analysis, and consequences for geothermometry. Amer Jour Sci 283A: 29-71

Fisk MR, Bence AE (1980) Experimental crystallization of chrome spinel in Famous basalt 527-1-1. Earth Planet Sci 48: 111-123

Ghiorso MS, Sack RO (1995) Chemical mass transfer in magmatic processes IV. A revised and internally consistent thermodynamic model for the interpolation and extrapolation of liquid–solid equilibria in magmatic systems at elevated temperatures and pressures. Contrib Mineral Petrol 119: 197-212

Grove TL (1993) Corrections to expressions for calculating mineral components in "Origin of Calc-Alkaline Series Lavas at Medicine Lake Volcano by Fractionation, Assimilation and Mixing" and "Experimental Petrology of normal MORB near the Kane Fracture Zone: 22o-25oN, mid-Atlantic ridge". Contrib Mineral Petrol 114: 422-424

Grove TL, Kinzler RJ, Bryan WB (1992) Fractionation of Mid-Ocean Ridge Basalt (MORB). In: Morgan JP, Blackman DK, Sinton JM (eds) Mantle flow and melt generation at Mid-Ocean Ridges. Geophys Monograph 71: 281-310, Washington, DC: American Geophysical Union

Hamilton MA, Pearson DG, Thompson RN, Kelly SP, Emeleus CH (1998) Rapid eruption of Skye lavas inferred from precise U-Pb and Ar-Ar dating of the Rum and Cuillin plutonic complexes. Nature 394: 260-263

Heber VS, Brooker RA, Kelley SP, Wood BJ (2007) Crystal-melt partitioning of noble gases (helium, neon, argon, krypton, and xenon) for olivine and clinopyroxene. Geochim Cosmochim Ac 71: 1041-1061

Hémond C, Arndt NT, Lichtenstein U, Hofman AW (1993) The heterogeneous Iceland plume: Nd-Sr-O isotopes and trace element constraints. J Geophys Res 98 (B9): 15833-15850

Henderson P (1975) Reaction trends shown by chrome-spinels of the Rhum layered intrusion. Geochim Cosmochim Ac 39: 1035-1044

Henderson P, Suddaby P (1971) The nature and origin of the chrome-spinel of the Rhum Layered Intrusion. Contrib Mineral Petrol 33: 21-31

Henderson P, Wood RJ (1981) Reaction relationships of chrome-spinels in igneous rocks – Further evidence from the Layered Intrusions of Rhum and Mull, Inner Hebrides, Scotland. Contrib Mineral Petrol 78: 225-229

Hildreth W, Moorbath S (1988) Crustal contributions to arc magmatism in the Andes of Central Chile. Contrib Mineral Petrol 98: 455-489

Hill R, Roeder P (1974) The crystallization of spinel from basaltic liquid as a function of Oxygen fugacity. J Geol 82 (6): 709-729

Holness MB (1999) Contact metamorphism and anatexis of Torridonian arkose by minor intrusions of the Rum Igneous Complex, Inner Hebrides, Scotland. Geol Mag 136: 527-542

Holness MB, Hallworth MA, Woods A, Sides RE (2007) Infiltration Metasomatism of Cumulates by Intrusive Magma Replenishment: the Wavy Horizon, Isle of Rum, Scotland. J Petrol 48(3): 563-587

Irvine (1965) Chromian spinel as a petrogenetic indicator. Part 1, Theory. Can J Earth Sci 2: 648-672

Irvine TN (1967) Chromian spinel as a petrogenetic indicator. Part 2, Petrologic applications. Can J Earth Sci 4: 71-103

Irvine TN (1975) Crystallization sequences in the Muskox intrusion and other layered intrusions – II. Origin of chromitite layers and similar deposits of the magmatic ores. Geochim Cosmochim Ac 39: 991-1020

Irvine TN (1977) Origin of chromite layers in the Muskox intrusion and other stratiform intrusions: a new perspective. Geology 5, 273-277

Irvine TN (1980) Magmatic infiltration metasomatism, double-diffusive fractional crystallization, and adcumulus growth in the Muskox intrusion and other layered intrusions. In: Hagraves RB (ed) Physics of Magmatic Processes. Princeton University Press, New Jersey, pp 325-383

Irvine TN (1982) Terminology for layered intrusions. J Petrol 23 (2): 127-162

Jakobsen JK, Veksler IV, Tegner C, Brooks CK (2005) Immiscible iron- and silica-rich melts in basalt petrogenesis documented in the Skaergaard intrusion. Geology 33: 885-888

Kamenetsky VS, Crawford AJ, Meffre S (2001) Factors controlling chemistry of magmatic spinel: an empirical study of associated olivine, Cr-spinel and melt inclusions fro primitive rocks. J Petrol 42 (4): 655-671

Kent RW (1995) Magnesian basalts from the Hebrides, Scotland: chemical composition and relationship to the Iceland plume. J Geol Soc 152:979–983

Kerr AC, Kent RW, Thomson BA, Seedhouse JK, Donaldson CH (1999) Geochemical evolution of the Tertiary Mull volcano, western Scotland. J Petrol 40: 873–908

Kress VC, Carmichael ISE (1991) The compressibility of silicate liquids containing Fe_2O_3 and the effect of composition, temperature, oxygen fugacity and pressure on their redox state. Contrib Mineral Petrol 108: 82-92

Kuritani T (1998) Boundary layer crystallization in a basaltic magma chamber: Evidence from Rishiri volcano, northern Japan. J Petrol 39(9): 1619-1640

Latypov R, O'Driscoll B, Lavrenchuk A (2013) Towards a model for the in situ origin of PGE reefs in layered intrusions: insights from chromitites seams of the Rum Eastern Layered Intrusion, Scotland. Contrib Mineral Petrol 166: 309-327

Lenaz D, O'Driscoll B, Princivalle F (2011) Petrogenesis of the anorthosite-chromitite association: crystal-chemical and petrological insights from the Rum Layered Suite, NW Scotland. Contrib Mineral Petrol 162: 1201-1213

Leuthold J, Blundy JD, Holness MB, Sides R (2014a) Successive episodes of reactive liquid flow through a layered intrusion (Unit 9, Rum Eastern Layered Intrusion, Scotland). Contrib Mineral Petrol 167:1021

Leuthold J, Müntener O, Baumgartner LP, Putlitz B (2014b) Petrological constraints on the recycling of mafic crystal mushes and intrusion of braided sills in the Torres del Paine mafic complex (Patagonia). J Petrol 55(5): 917-949

Leuthold J, Müntener O, Baumgartner LP, Putlitz B, Ovtcharova M, Schaltegger U (2012) Time resolved construction of a bimodal laccolith (Torres del Paine, Patagonia). Earth Planet Sci Let 325-326: 85-92

Lipin BR (1993) Pressure increase, the formation of chromite seams, and the development of the ultramafic serie in the Stillwater Complex, Montana. J Petrol 34(5): 955-976

Manoochehri S, Schmidt MW (2014) Settling and compaction of chromite cumulates employing a centrifuging piston cylinder and application to layered mafic intrusions. Contrib Mineral Petrol 168: 1091

McClurg J (1982) Geology and structure of the northern part of the Rhum ultrabasic complex. University of Edinburgh, PhD thesis (unpublished)

McDonald JA (1965) Liquid immiscibility as one factor in chromitite seam formation in the Bushveld Igneous Complex. Econ Geol Bull Soc 60: 1674-1685

Mills RD, Glazner AF (2013) Experimental study on the effect of temperature cycling on coarsening of plagioclase and olivine in an alkali basalt. Contrib Mineral Petrol 166: 97-111

Mills RD, Ratner JJ, Glazner AF (2011) Experimental evidence for crystal coarsening and fabric development during temperature cycling. Geology 39: 1139-1142

Morse SA (1980) Basalts and phase diagrams: an introduction to the quantitative use of phase diagrams in igneous petrology. Springer, p 493

Murck BW, Campbell IH (1986) The effects of temperature, oxygen fugacity and melt composition on the behaviour of chromium in basic and ultrabasic melts. Geochim Cosmochim Ac 50: 1871-1887

O'Driscoll B, Day JMD, Daly JS, Walker RJ, McDonough WF (2009a) Rhenium-osmium isotopes and platinium-group elements in the Rum Layered Suite, Scotland: Implications for the Cr-spinel seam formation and the composition of the Iceland mantle anomaly. *Earth Planet Sci Let* **286**: 41-51.

O'Driscoll B, Donaldson CH, Daly JS, Emeleus CH (2009b) The roles of melt infiltration and cumulate assimilation in the formation of anorthosite and a Cr-Spl seam in the Rum Eastern Layered Intrusion, NW Scotland. Lithos 111: 6-20

O'Driscoll B, Emeleus CH, Donaldson CH, Daly JS (2010) Cr-spinel seam petrogenesis in the Rum layered suite, NW Scotland: Cumulate assimilation and in situ crystallization in a deforming crystal mush. J Petrol 51(6): 1171-1201

O'Driscoll B, Hargraves RB, Emeleus CH, Troll VR, Donaldson CH, Reavy RJ (2007) Magmatic lineations inferred from anisotropy of magmatic susceptibility fabrics in Units 8, 9, and 10 of the Rum Eastern Layered Series, NW Scotland. Lithos 98, 27-44

O'Hara, M.J., and Herzberg, C., 2002, Interpretation of trace element and isotope features of basalts: Relevance of fi eld relations, petrology, major element data, phase equilibria, and magma chamber modeling in basalt petrogenesis: Geochem. Cosmochem Ac. 66: 2167–2191.

Ozawa K (1984) Olivine-spinel geospeedometry: analysis of diffusion-controlled Mg-Fe^{2+} exchange. Geochim Cosmochim Ac 48: 2597-2611

Palacz ZA, Tait SR (1985) Isotopic and geochemical investigation of Unit 10 from the Eastern Layered Series of the Rhum intrusion, Northwest Scotland. Geol Mag 122 (5): 485-490

Power MR, Duncan P, Andersen JCØ, Wheeler PD (2000) Testing the validity of chrome spinel chemistry as a provenance and petrogenetic indicator. Geology 28: 1027-1030

Princivalle F, Della Giusta A, De Min A, Piccirillo EM (1999) Crystal chemistry and significance of cation ordering in Mg-Al rich spinels from high grade hornfels (Predazzo-Monzoni, NE Italy). Mineral Mag 63:257–262

Putnis A, Price GD (1979) The nature and significance of exsolved phases in some chrome spinels from the Rhum layered intrusion. Mineral Mag 43: 519-526

Renna MR, Tribuzio R (2011) Olivine-rich troctolites from Ligurian ophiolites (Italy): Evidence for impregnation of replacive mantle conduits by MORB-type melts. J Petrol 52(9): 1763-1790

Renner R, Palacz Z (1987) Basaltic replenishment of the Rhum magma chamber: evidence from unit 14. J Geol Soc London 144: 961-970

Ridley WI (1977) The crystallization trends of spinels in the Tertiary basalts from Rhum and Muck and their petrogenetic significance. Contrib Mineral Petrol 64: 243-255

Roeder PL (1994) Chromite: from the fiery rain of chondrules to the Kilauea Iki lava lake. Can Mineral 32: 729-746

Roeder PL, Campbell IH, Jamieson HE (1979) A re-evaluation of the olivine-spinel geothermometer. Contrib Mineral Petrol 68: 325-334

Roeder PL Reynolds I (1991) Crystallization of chromite and chromium solubility in basaltic melts. J Petrol 32(5): 909-934

Roeder PL, Poustovetov A, Oskarsson N (2001) Growth forms and composition of chromian spinel in MORB magma: Diffusion-controlled crystallization of chomian spinel. Can Mineral 39: 397-416

Saint Blanquat M, Horsman E, Habert G, Morgan S, Vanderhaeghe O, Law R, Tikoff B (2011) Multiscale magmatic cyclicity, duration of pluton construction, and the paradoxical relationship between tectonism and plutonism in continental arcs. Tectonophysics 500: 20-33

Saunders AD, Fitton JG, Kerr AC, Norry MJ, Kent RW (1997) The North Atlantic igneous province. In Mahoney JJ, Coffin MF (ed) Large igneous provinces: Continental, oceanic, and planetary flood volcanism, American Geophysical Union, Washington, pp 45-93

Scowen PAH, Roeder PL, Helz RT (1991) Reequilibration of chomite within Kilauea Iki lava lake, Hawaii. Contrib Mineral Petrol 107: 8-20

Sharpe MR, Irvine TN (1983) Melting relations of two Bushveld chilled margin rocks and implications for the origin of chomitite. Carnegie Inst Wash Yearb 82: 295-300

Sisson TW, Grove TL (1993a) Experimental investigations of the role of H_2O in calc-alkaline differentiation and subduction zone magmatism. Contrib Mineral Petrol 113: 143-166

Sisson TW, Grove TL (1993b) Temperatures and H_2O contents of low-MgO high-alumina basalts. Contrib Mineral Petrol 113: 167-184

Solano J.M.S., Jackson M.D., Sparks R.S.J., Blundy J.D., Annen C. (2012). Melt segregation in deep crustal hot zones: a mechanism for chemical differentiation, crustal assimilation and the formation of evolved magmas. J Petrol 53(10): 1999-2026.

Soulard H, Boivin P, Libourel G (1994) Liquid-forsterite-anorthite-spinel assemblage at 1 bar in the CMAS system: implications for low-pressure evolution of high-Al and high-Mg magmas. Eur J Mineral 6(5): 633-646

Suzuki AM, Yasuda A, Ozawa K (2008) Cr and Al diffusion in chromite spiel: Experimental determination and its implication for diffusion creep. Phys Chem Minerals 35: 433-445

Tepley FJ, Davidson JP (2003) Mineral-scale Sr-isotope constraints on magma evolution and chamber dynamics in the Rum layered intrusion, Scotland. Contrib Mineral Petrol 145: 628-641

Thy P (1983) Spinel minerals in transitional and alkali basaltic glasses from Iceland. Contrib Mineral Petrol 83: 141-149

Thy P, Lesher CE, Nielsen TFD, Brooks CK (2006) Experimental constraints on the Skaergaard liquid line of descent. Lithos 92 : 154-180

Toplis MJ, Carroll MR (1995) An experimental study of the influence of oxygen fugacity on Fe-Ti oxide stability, phase relations, and mineral-melt equilibria in ferro-basaltic systems. J Petrol 36: 1137–1170

Tronnes RG (1990) Basaltic melt evolution of the Hengill Volcanic System, SW Iceland, and evidence for clinopyroxene assimilation in primitive tholeiitic magmas. J Geophy Res 95(B10) : 15893-15910

Ulmer GC (1969) Experimental investigations of chromite spinels. Econ Geol Monogr 4: 114-131

Upton BGJ, Skovgaard AC, McClurg J, Kirstein L, Cheadle M, Emeleus CH, Wadsworth WJ, Fallick AE (2002) Picritic magmas and the Rum ultramafic complex, Scotland. Geol Mag 139: 437-452

Wilke M, Behrens H (1999) The dependence of the partitioning of iron and europium between plagioclase and hydrous tonalitic melt on oxygen fugacity. Contrib Mineral Petrol 137: 102-114

Wilson AH (1982) The geology of the Great 'Dyke', Zimbabwe: The ultramafic rocks. J Petrol 23(2): 240-292

Young IM (1984) Mixing of supernatant and interstitial fluids in the Rhum layered intrusion. Mineral Mag 48: 345-350

Figure captions:

Figure 1: Schematic representation of the complex reactive liquid flow process (modified from Leuthold et al., 2014). Percolation of reactive liquid within crystal mush/cumulate has important consequences: crystal chemistry and textures are modified by dissolution-recrystallization and re-equilibration; the rock structure is changed by compaction and modification of the mineral mode; and the percolating liquid chemistry is modified by assimilation, mixing and mingling, perturbing the normal liquid line of descent.

Figure 2: Experimentally-determined liquid compositions. Picrite 1atm, anhydrous, QFM; MELTS (Ghiorso and Sack, 1995; Asimow and Ghiorso, 1998) calculations and Rum aphyric dykes are shown for reference. B62/2 picrite and 11JL33 basalt were used as starting material in the experiments. Grey areas delimit the composition of Iceland plume mafic lavas (Hémond et al., 1993). The Rum picrite liquid line of descent is very similar to the trend defined by the Rum dykes and Icelandic alkaline basalt. Through clinopyroxene-rich cumulate assimilation, the experimental glass SiO_2 content is distinctly increased. Through clinopyroxene- and/or olivine-rich cumulate assimilation, the liquid Mg# is increased. [1]McClurg, 1982 unpublished PhD thesis, [2]Leuthold et al., 2014a

Figure 3: BSE images of representative experimental run products (see Tables 2 to 5 for conditions). a) Picrite at 1210°C, QFM (run#87), illustrating few olivine and Cr-spinel crystals. Spinel grains are ~3µm in diameter and require high spatial-resolution FEG-EMPA analysis. b) Picrite at 1170°C, QFM (run#51), showing the first occurrence of clinopyroxene. c) Picrite at 1125°C, QFM (run #63), with 30 vol% glass. Crystallization of large euhedral crystals in figures *b* and *c* was achieved by slow cooling (Heber et al., 2007) and temperature oscillation (Mills et al., 2011; Mills and Gardner, 2013). The mineral modes in slowly cooled experiments are indistinguishable from isothermal experiments. Olivine crystals show zoning (especially at low temperature). d) Picrite-troctolite hybrid (50-50%) at 1190°C, QFM (run #78). The melt fraction is lower than in picrite at similar temperatures. Cr-spinel mode is higher than in picrite and clinopyroxene saturation temperature is lowered to ~1160°C. e) Picrite at 1180°C, QFM+2.8 (run #99). Under more oxidized conditions, spinel mode is enhanced and its composition is more Fe^{3+}-rich. f) Picrite at 1180°C, QFM-2.2 (run #61). Under more reducing conditions, spinel is distinctly Fe^{3+}-poor and becomes unstable at high temperature, as evidenced by corroded texture. Abbreviations: Ol: olivine; Cr-spl: Cr-spinel; Plg: plagioclase; Cpx: clinopyroxene. Scale bar is 100µm.

Figure 4: Schematic representation of equilibrium mineral parageneses (filled grey fields in boxes) in picrite (B62/2, Upton et al., 2002) (QFM+1.8, QFM and QFM-2.2), picrite-troctolite, picrite-gabbro and gabbro experiments (see Table 1 for starting compositions and Tables 2 to 5 for run conditions and modal abundances), as a function of temperature and Mg# of starting material. Spinel is stable in most experiments. Cr-spl: Cr and Al-spinel; Spl: magnetite and titanomagnetite Ol: olivine; Plg: plagioclase; Cpx: clinopyroxene.

Figure 5: Mineral mode (vol%) in 0.1 MPa experiments. The liquid fraction is high until plagioclase fractionation starts and strongly decreases thereafter. Clinopyroxene saturation temperature is systematically lower than plagioclase one. Calculations using the MELTS (Ghiorso and Sack, 1995; Asimow and Ghiorso,

1998) algorithm at identical conditions show a good correspondence in mineral modes and saturation temperatures. Modal estimates have uncertainties of less than ±5 vol%.

Figure 6: Glass and mineral chemistry as a function of temperature. The vertical bars indicate the variation of mineral compositions of Rum aphyric dykes and Unit 9 minerals (data from Holness et al., 2007 and Leuthold et al., 2014a). Spinel, olivine and clinopyroxene chemistry is strongly dependent on fO_2. At identical temperature (i.e. lower melt fractions), the plagioclase anorthite content is higher in hybrid picrite-troctolite and picrite-gabbro experiments compared to picrite experiments. High temperature olivine and clinopyroxene (when present) have a higher Mg# in hybrid experiments. [1]McClurg (1982, unpublished PhD thesis), [2]Leuthold et al. (2014a), [3]Holness et al. (2007)

Figure 7: Spinel chemistry (averaged compositions). a) Fe# (Fe# = $Fe^{2+}/[Mg+Fe^{2+}]$) progressively increases upon cooling, while Al/(Cr+Al) decreases. The experimental data reveal systematically higher Al/(Cr+Al) than the Rum Unit 9 grains. Spinel chemistry in picrite-troctolite experiments is highly variable in Al/(Cr+Al), ranging from low ratio at high temperature to higher ratio than in picrite experiments at intermediate temperature. Through rapid re-equilibration with olivine down to sub-solidus conditions, spinel becomes Fe^{2+}-rich and Mg-poor (Roeder et al., 1979; Scowen et al., 1991; Kamenetsky et al., 2001, O'Driscoll et al., 2010). b) Down-temperature, spinel becomes Ti-rich. Prior to plagioclase saturation, spinel Al-content increases slightly. Spinels crystallized from Ti-poor and Al-rich hybrid melts have lower Ti and higher Al contents than spinels in picrite experiments (at the same melt fraction). [1]Holness et al. (2007), [2]Leuthold et al. (2014b), [3]O'Driscoll et al. (2009b), [4]O'Driscoll et al. (2010), [5]Upton et al. (2002)

Figure 8: Spinel trivalent cations chemistry (individual analyses). a) Natural spinels from the Rum Eastern Layered Intrusion (Units 7-8 and 11-12 boundaries, Unit 9 and picritic dykes [M9 and B62/2]) (modified after Leuthold et al., 2014 and O'Driscoll et al., 2010 and references therein). b) Calculations using MELTS (Ghiorso and Sack, 1995; Asimow and Ghiorso, 1998) covering a wide range of P-T-X-fO_2 conditions at which the Rum cumulates may have formed. QFM and oxidized picrite fail to reproduce the Rum Unit 9 Cr-rich spinels. Intermediate temperature spinel crystallized under reduced conditions should have high Cr#. Fractional crystallization, especially under reduced conditions, produces higher Cr# spinel. The Al/(Al+Cr) ratio is lowered when the fO_2 is left free. Spinel crystallizing at moderate pressure or from hydrous melt results in even lower Cr#. Picrite-troctolite and plagioclase-doped picrite (not shown) spinels show a large Al/(Cr+Al) scatter. Fractional crystallization under reduced conditions best reproduces the Unit 9 chromite. High temperature Cr-rich spinels are absent along the basalt liquid line of descent. c) Spinel equilibrated at 0.1 MPa from anhydrous picritic liquid variously affected by hybridization with mafic cumulate (gabbro, troctolite) (see Table 1 for compositions). Along the picritic liquid line of descent, spinel Al_2O_3 concentration increases up to the point of plagioclase saturation. Upon plagioclase crystallization, spinel Cr# increases until clinopyroxene saturates. With subsequent cooling, spinel rapidly evolves to magnetite and titanomagnetite compositions. Abundant Fe^{3+}-rich spinel crystallizes under oxidized conditions. Conversely, Fe^{3+}-poor spinel is rare under reduced conditions and becomes unstable following clinopyroxene saturation. Gabbro assimilation results in very limited variation of Cr-spinel chemistry during cooling. In contrast, troctolite assimilation strongly modifies spinel chemistry,

generating Al-rich spinels at high temperature, Cr-rich spinel at ~1180°C and Fe^{3+}-rich spinels at lower temperature. The Rum Unit 9 chromites are best reproduced by picrite-troctolite experiments at 1180°C, QFM-1.2. Selected experimental temperatures [°C] are shown for reference. The grey shaded area delimits the Rum Unit 9 Cr-spinel compositional field. [1]Holness et al. (2007), [2]Leuthold et al. (2014a), [3]O'Driscoll et al. (2009b), [4]O'Driscoll et al. (2010), [5]Dunham and Wilkinson (1985), [6]Upton et al. (2002).

Figure 9: BSE image and Al and Cr X-ray maps of the interface between a synthetic picrite and a troctolite initially equilibrated at 1250°C and QFM-1.2, left to react for 5 hours at similar conditions (run #154). Note the high abundance of Al- and Cr-spinel (up to 3.5 vol%) in the troctolite side of the hybrid reaction zone, where plagioclase is absent.

Figure 10: Schematic diagram illustrating potential modification of Cr-spinel chemistry by common magmatic processes. The diamond symbol indicates the Cr-spinel composition crystallized from B62/2 picrite starting material at 1180°C, QFM. The arrows show isothermal chemistry modifications and will change according to different temperatures (e.g. hot mafic, intermediate or cool differentiated interstitial melt). See text for discussions and references. [1]Henderson (1975), [2]Bell and Claydon (1992).

Appendix figure 1: Geological map of the Hallival region, Eastern Layered Intrusion (ELI), from Emeleus (2004) (WLI: Western Layered Intrusion; CC: Central Complex). Units 8, 9, 10 and 11 allivalite are indicated. Note the discontinuous nature of the Unit 9 peridotite, attributed to formation from a sill-like intrusion of picrite (Bédard et al. 1988). Traverses F, G, H and E show the location of the traverses of Holness et al. (2007). Traverse M and its surroundings were described by Sides (2008, unpublished PhD thesis) and Leuthold et al. (2014a). Unit 7-8 and 11-12 boundaries were studied by O'Driscoll et al. (2009b, 2010). The brown cross in the inset shows the location of picritic dyke B62/2 sampled by McClurg (1982, unpublished PhD thesis) and analysed by Upton et al. (2002).

Appendix figure 2: Schematic examples of different experimental cooling paths used. Isothermal experiments (a,b) were set at the equilibrium conditions and quenched. The goal was to accurately determine the phase assemblage, proportions and major element chemistry. We used temperature oscillation (generally ±10°C) to grow coarser crystals with fewer inclusions, following Mills et al. (2011) and Mills and Gardner (2013). Following Fisk and Bence (1980), we ran cooling-rate experiments (c,d,e,f) to grow large crystals. Upon cooling, the fO_2 was constantly adjusted along a buffer. Crystals (mostly olivine ± clinopyroxene) in such experiments show little zoning, especially when equilibrated at low temperature ($F<0.4$). Undercooling was sometimes observed, evidenced by the absence of low temperature phases. In a few runs (c), samples were initially heated to 1260°C, where they became saturated in olivine and spinel, representing an already differentiated, crystal-bearing magma. Combining temperature oscillation to progressive cooling (e,f) contributes to growth of even larger crystals. Temperature oscillation (±10°C) 15°C below the saturation temperature of a new phase (f) is especially efficient in growing large crystals.

Appendix figure 3: Picrite (1), picrite-troctolite (2) and picrite-gabbro (3) cotectic compositions and

temperatures, plotted in the Forsterite – Diopside – Anorthite ternary projection using the algorithm of Grove (1993). The clinopyroxene stability field increases at the expense of the plagioclase in hybrid picrite-gabbro experiments and is significantly decreased in picrite-troctolite experiments. Basalt, troctolite and gabbro liquidus glasses are shown for comparison.

Table 1: Composition of the Rum B62/2 picritic dyke (Upton et al., 2002), 11JL27 gabbro and 11JL16 troctolite (Leuthold et al., 2014a) that were mixed in different proportions to make the starting materials of our experiments.

Table 2: Run conditions and modal abundances from experiments on B62/2 picrite. Cooling paths are shown on the Appendix figure 2. The first 109 experiments were run at the University of Bristol. Experiments 110 to 182 were run at ETH Zürich.

Table 3: Run conditions and modal abundances from experiments using 11JL33 basalt.

Table 4: Run conditions and modal abundances from experiments using a 50:50 mix of B62/2 picrite + 11JL16 troctolite and 11JL16 troctolite.

Table 5: Run conditions and modal abundances from experiments using a 50:50 mix of B62/2 picrite + 11JL27 gabbro and 11JL27 gabbro.

Appendix table 1: Average experimental mineral and glass compositions, analysed by FEG-EMPA.

Appendix table 2: Individual glass and mineral analyses from picrite-troctolite kinetic experiment (reacted for 2h at 1250°C, QFM-1.2) (run #154).

Appendix table 3: Chemical comparison of natural olivine (forsterite content), plagioclase (anorthite content, Fe_2O_3) and clinopyroxene (Cr_2O_3, Al_2O_3, TiO_2) from Rum Unit 9 with experimental run products at different temperatures and fO_2 (based on Figure 6).

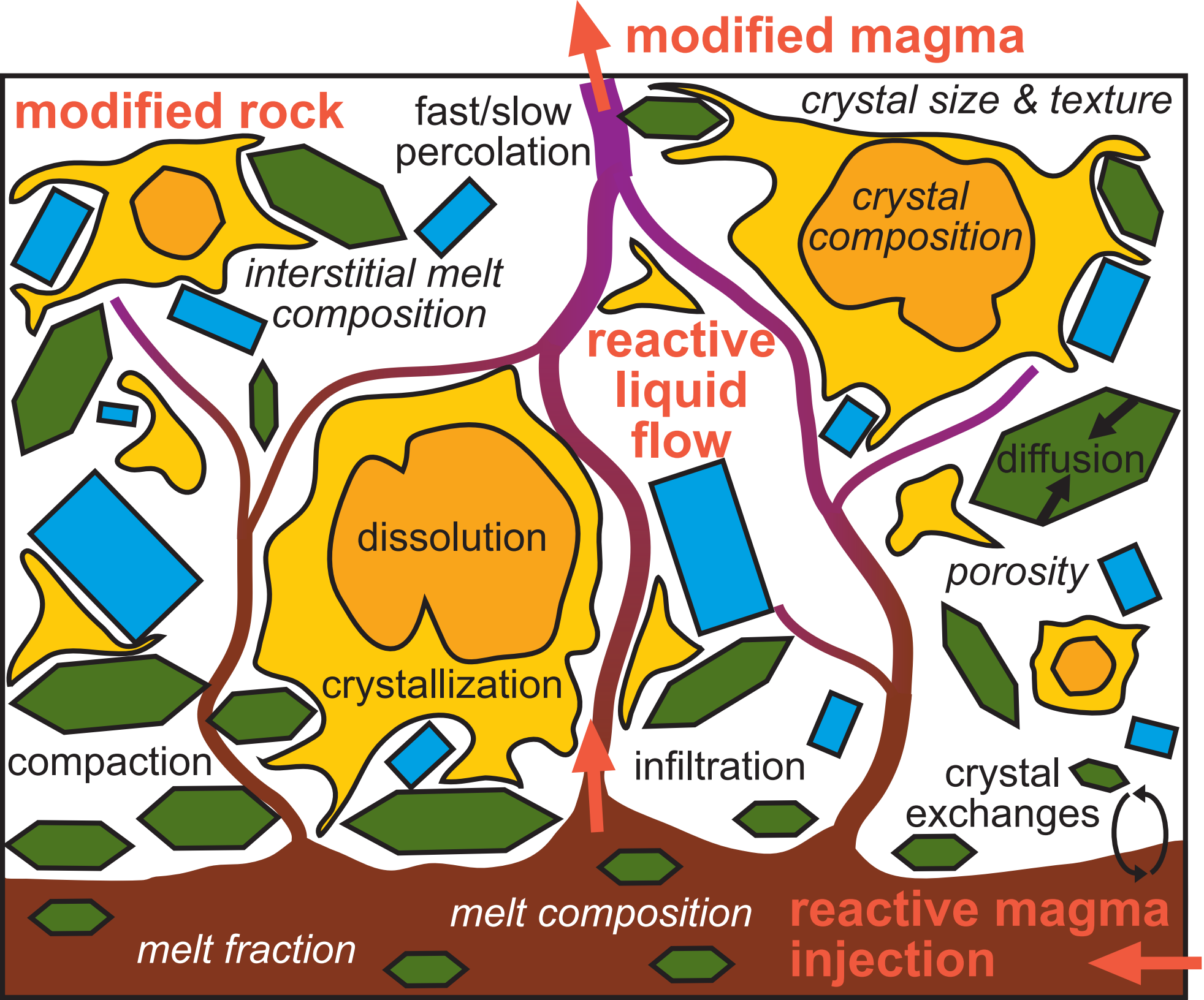

Figure1
Click here to download Figure: Fig1.eps

Figure2

Click here to download Figure: Fig2.eps

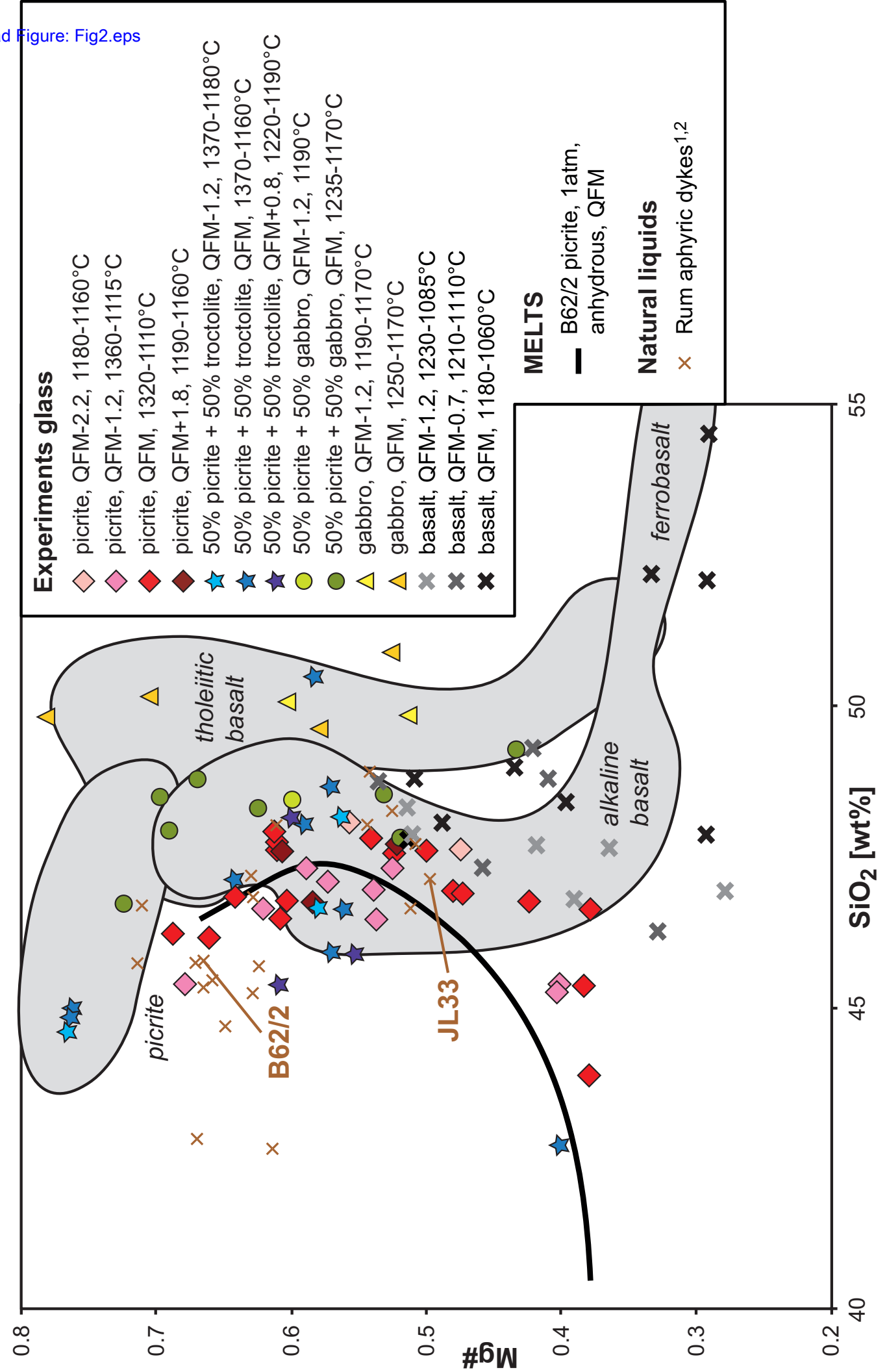

Figure3
Click here to download Figure: Fig3.tif

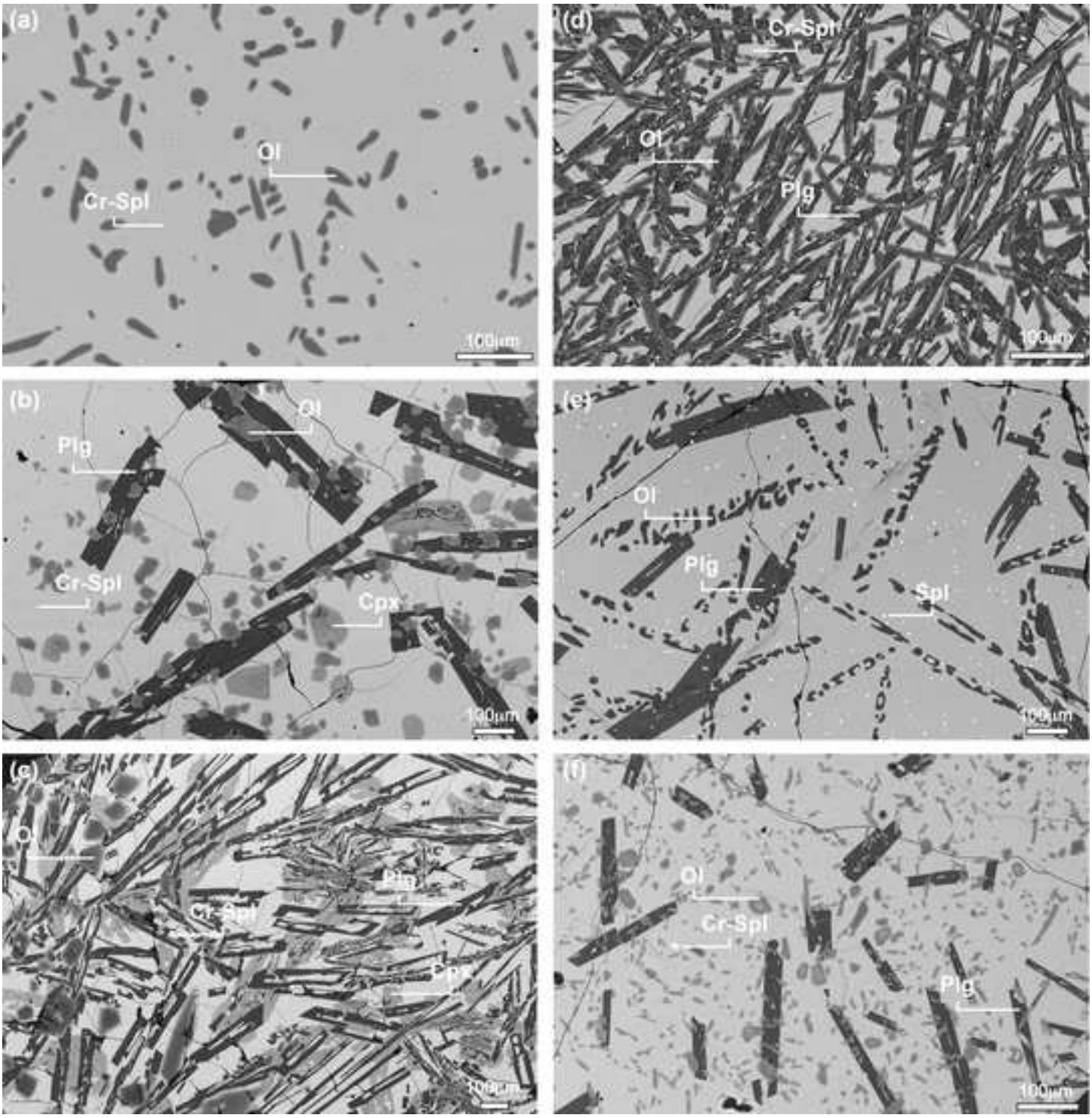

Figure4
Click here to download Figure: Fig4.eps

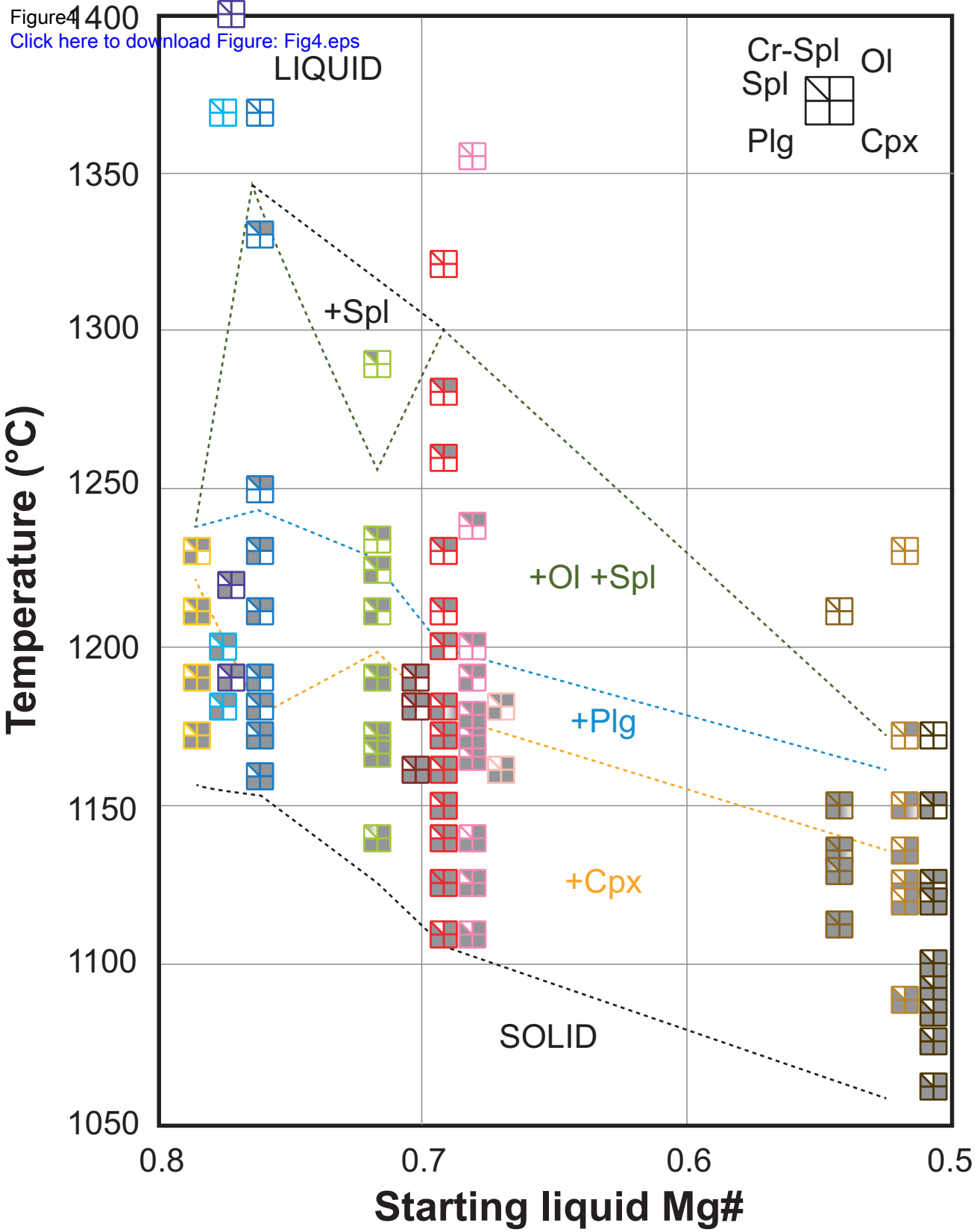

picrite, QFM-2.2
picrite, QFM-1.2
picrite, QFM
picrite, QFM+1.8
basalt, QFM-1.2
basalt, QFM-0.7
basalt, QFM
50% picrite + 50% troctolite, QFM-1.2
50% picrite + 50% troctolite, QFM
50% picrite + 50% troctolite, QFM+0.8
50% picrite + 50% gabbro, QFM
gabbro, QFM

Figure5
Click here to download Figure: Fig5.eps

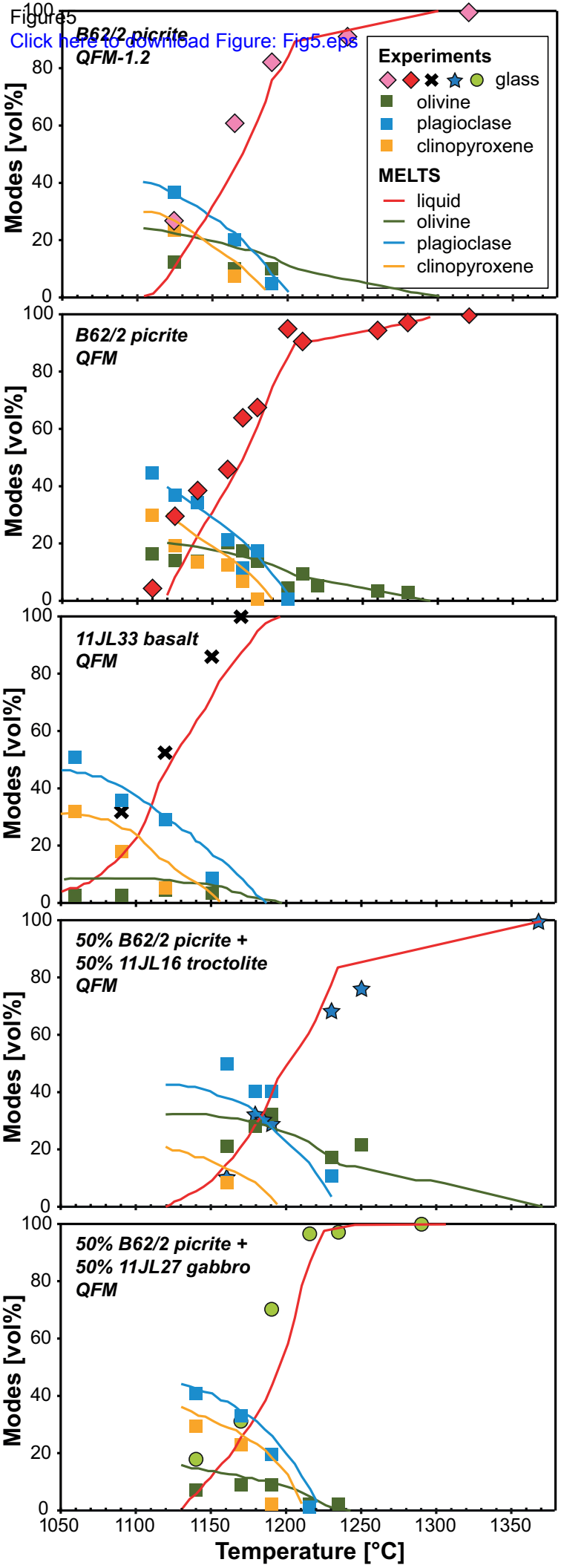

Figure6
Click here to download Figure: Fig6.eps

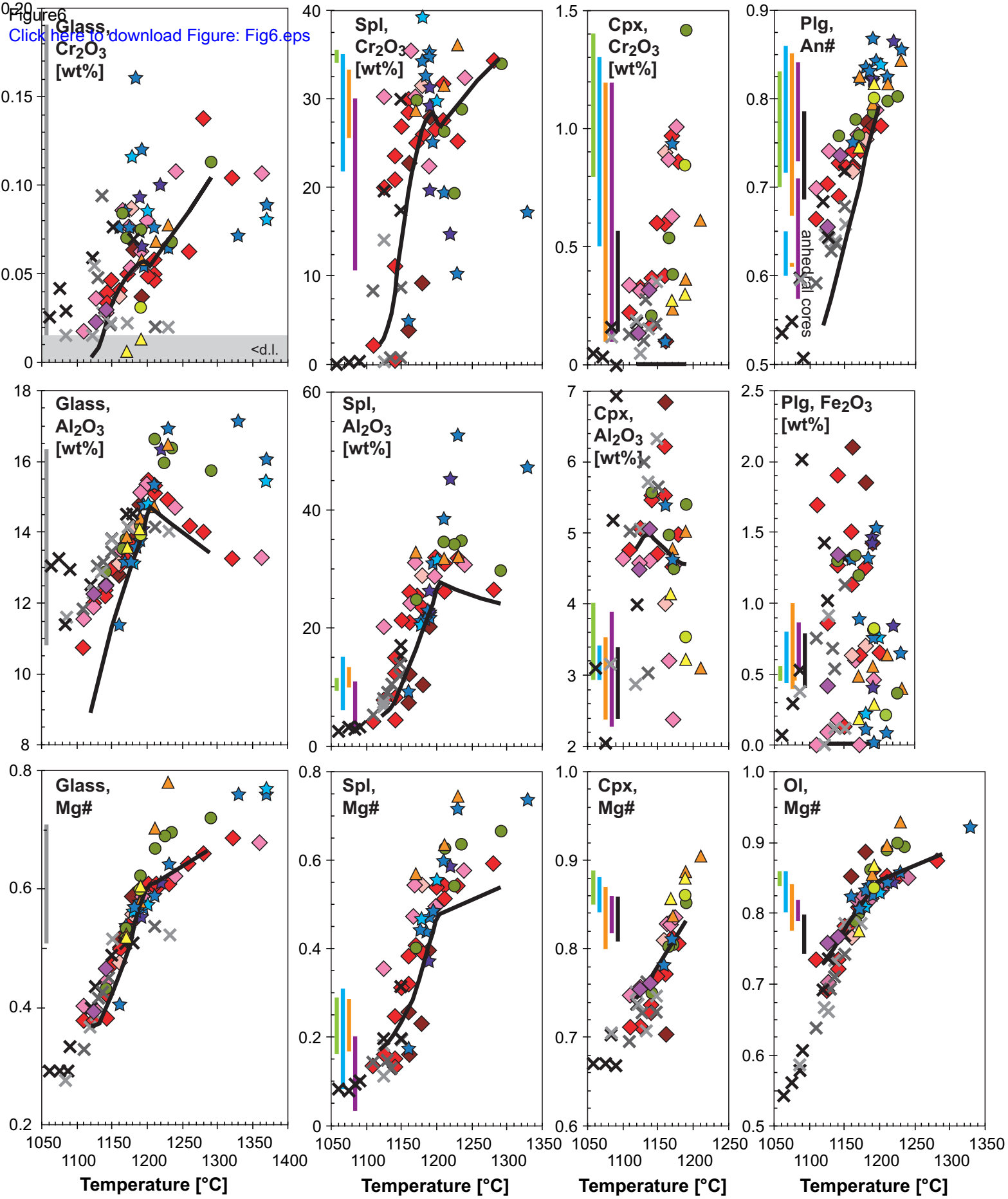

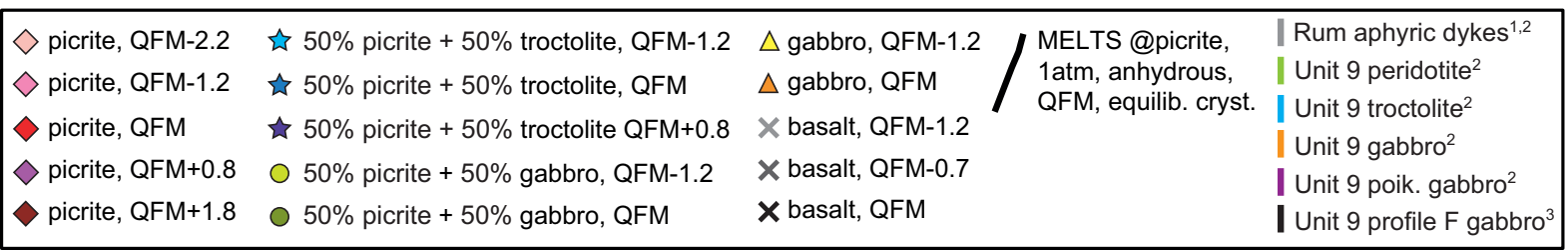

Figure7
Click here to download Figure: Fig7.eps

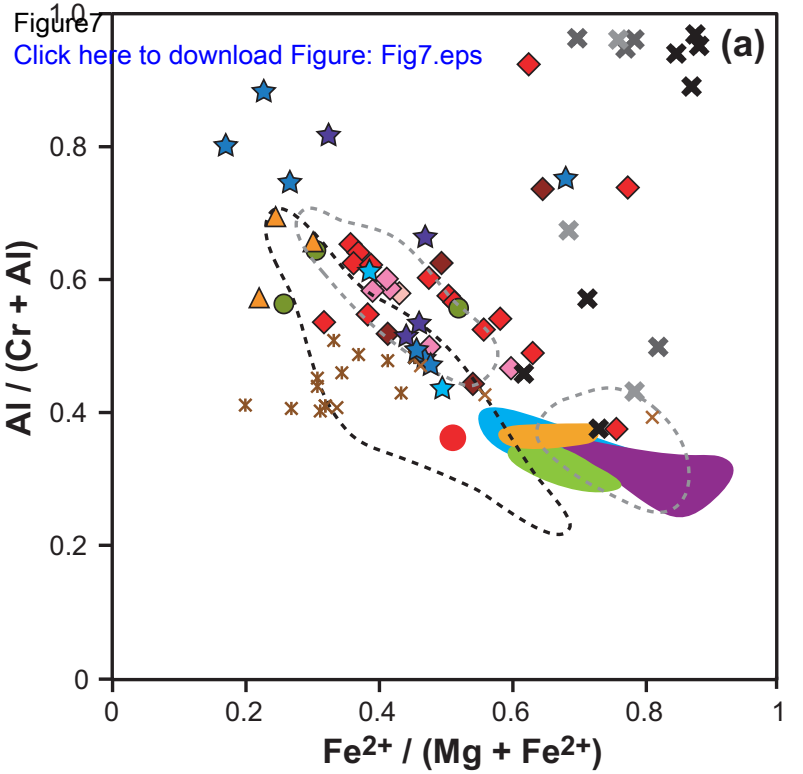

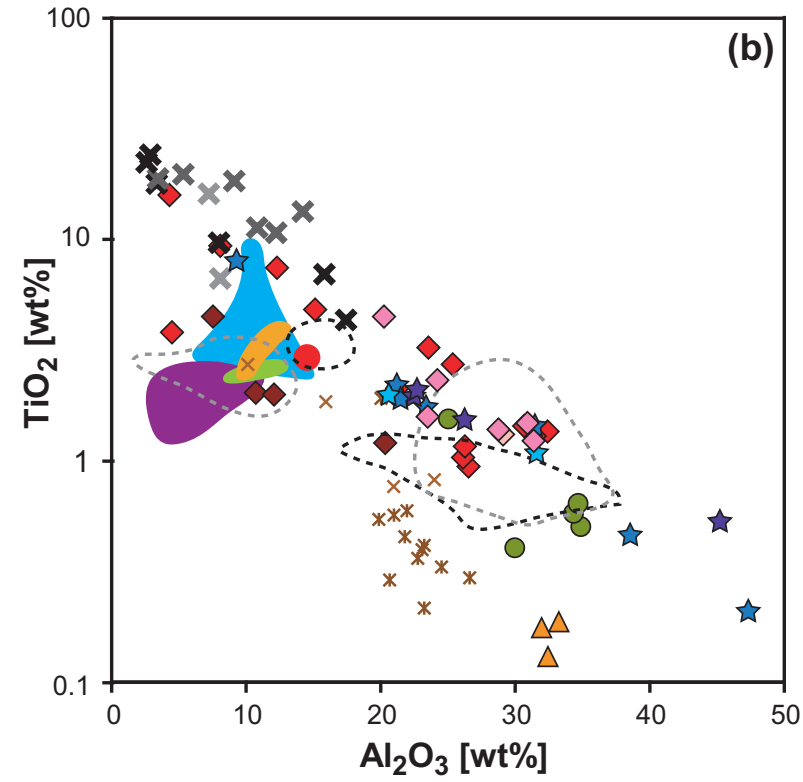

Experiments spinel

- picrite, QFM-2.2
- picrite, QFM-1.2
- picrite, QFM
- picrite, QFM+1.8
- picrite + troctolite, QFM-1.2
- picrite + troctolite, QFM
- picrite + troctolite, QFM+0.8
- picrite + gabbro, QFM
- gabbro, QFM
- basalt, QFM-1.2
- basalt, QFM-0.7
- basalt, QFM

Natural spinel

- Rum U9, peridotite [1,2]
- Rum U9, troctolite [1,2]
- Rum U9, gabbro [1,2]
- Rum U9, poik gabbro [2]
- Rum U9, anorthosite [2]
- U7-8 [3]
- U11-12 [4]
- Rum Ol-phyric picritic dyke (M9) [4,5]
- Rum Picritic dike [5]

Figure8

Click here to download Figure: Fig8.eps

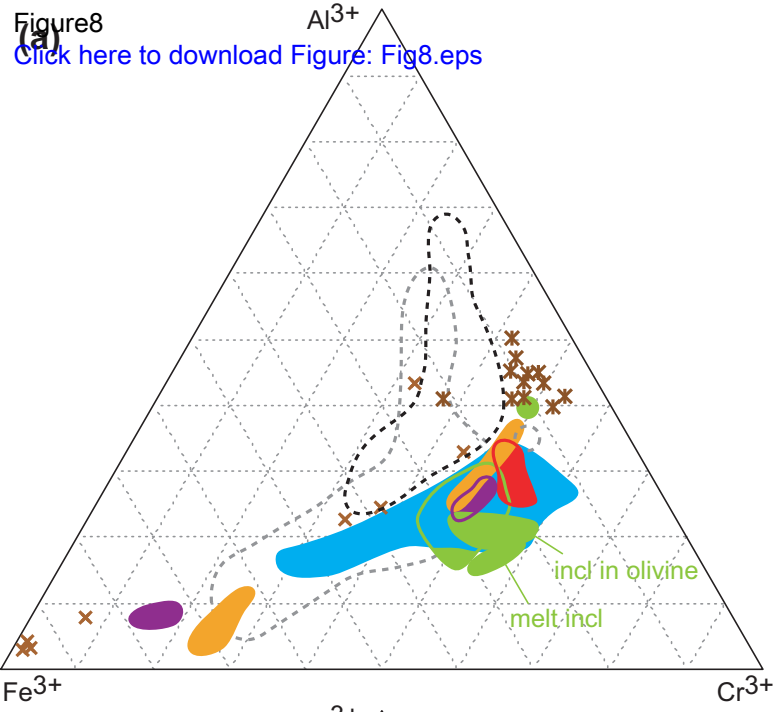

Natural crystals

- U9 peridotite [1,2]
- U9 Troctolite [1,2]
- U9 Gabbro [2]
- U9 Poikilitic gabbro [2]
- U9 Anorthosite [2]
- U7-8 (seam + dispersed) [3,4]
- U11-12 (seam + dispersed) [4,5]
- Ol-phyric picritic dyke (M9) [4,6]
- Picritic dike (B62/2) [6]

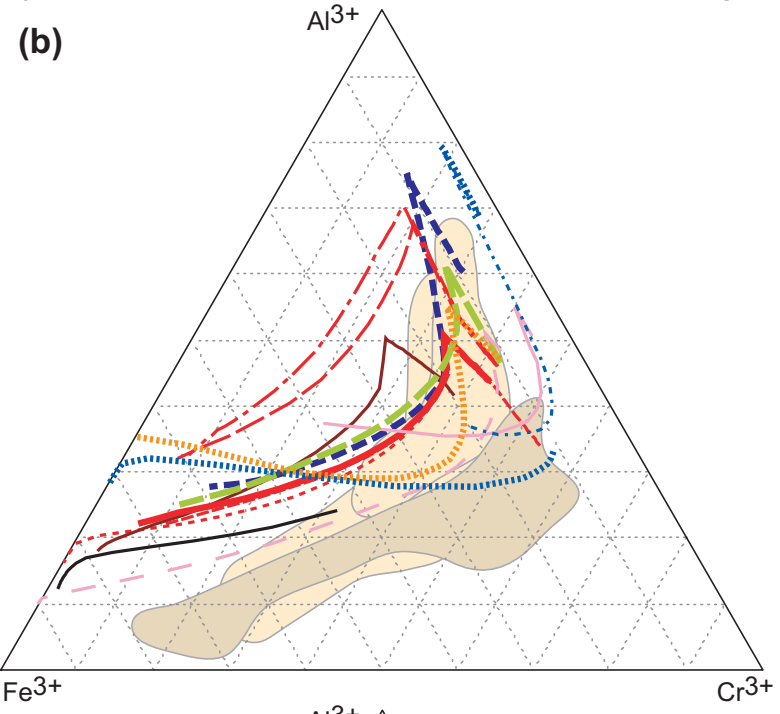

MELTS calculations

- 1atm, QFM, dry, B62/2 picrite
- 1atm, QFM, dry, B62/2 picrite, solid fractionation
- 1atm, QFM, dry, B62/2 picrite + 0.2wt% Cr_2O_3
- 1atm, QFM+0.8, dry, B62/2 picrite
- 1atm, QFM-2, dry, B62/2 picrite
- 1atm, QFM-2, dry, B62/2 picrite, solid fractionation
- 1atm, fO_2-free (initial QFM-1), dry, B62/2 picrite, solid fractionation
- 0.3GPa, QFM, dry, B62/2 picrite
- 0.3GPa, QFM, 0.2wt% H_2O, B62/2 picrite
- 1atm, QFM, dry, 50% B62/2 picrite + 50% 11JL16 troctolite
- 1atm, QFM-2, dry, 50% B62/2 picrite + 50% 11JL16 troctolite
- 1atm, QFM-2, dry, 50% B62/2 picrite + 50% 11JL16 troctolite, solid fractionation
- 1atm, QFM, dry, 50% B62/2 picrite + 50% 11JL27 gabbro
- 1atm, QFM, dry, 11JL33 basalt

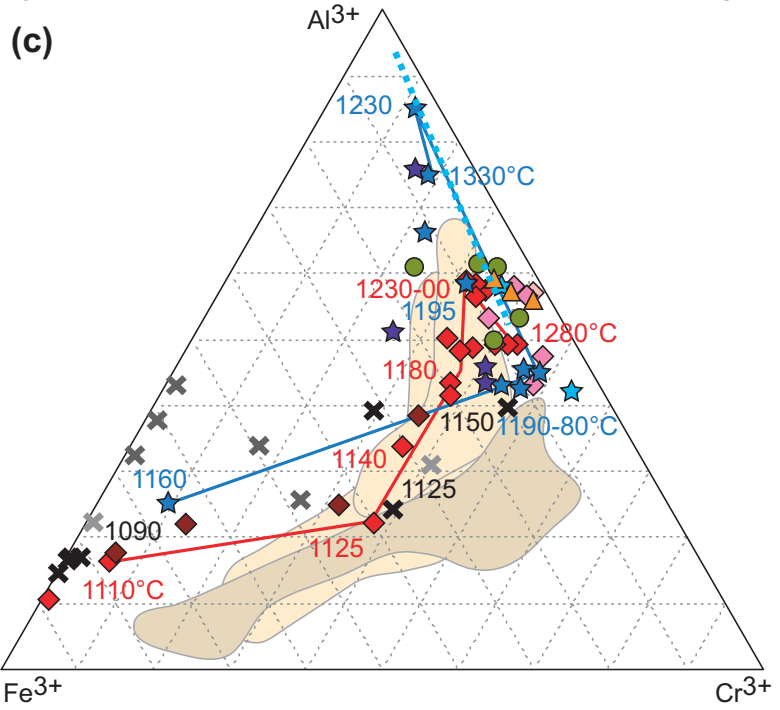

Experiments spinel

- picrite, QFM-2.2, 1180°C
- picrite, QFM-1.2, 1240-1125°C
- picrite, QFM, 1280-1110°C (cooling + equilibrium)
- picrite, QFM+1.8, 1190-1160°C
- 50% picrite + 50% troctolite, QFM-1.2, 1200-1180°C
- 50% picrite + 50% troctolite, QFM, 1330-1160°C
- 50% picrite + 50% troctolite QFM+0.8, 1220-1190°C
- 50% picrite + 50% gabbro, QFM, 1290-1170°C
- gabbro, QFM, 1230-1170°C
- basalt, QFM-1.2, 1125°C
- basalt, QFM-0.7, 1150-1130°C
- basalt, QFM, 1150-1060°C
- picrite-troctolite reaction, QFM-1.2, 1250°C, 5 hours

Figure9
Click here to download Figure: Fig9.tif

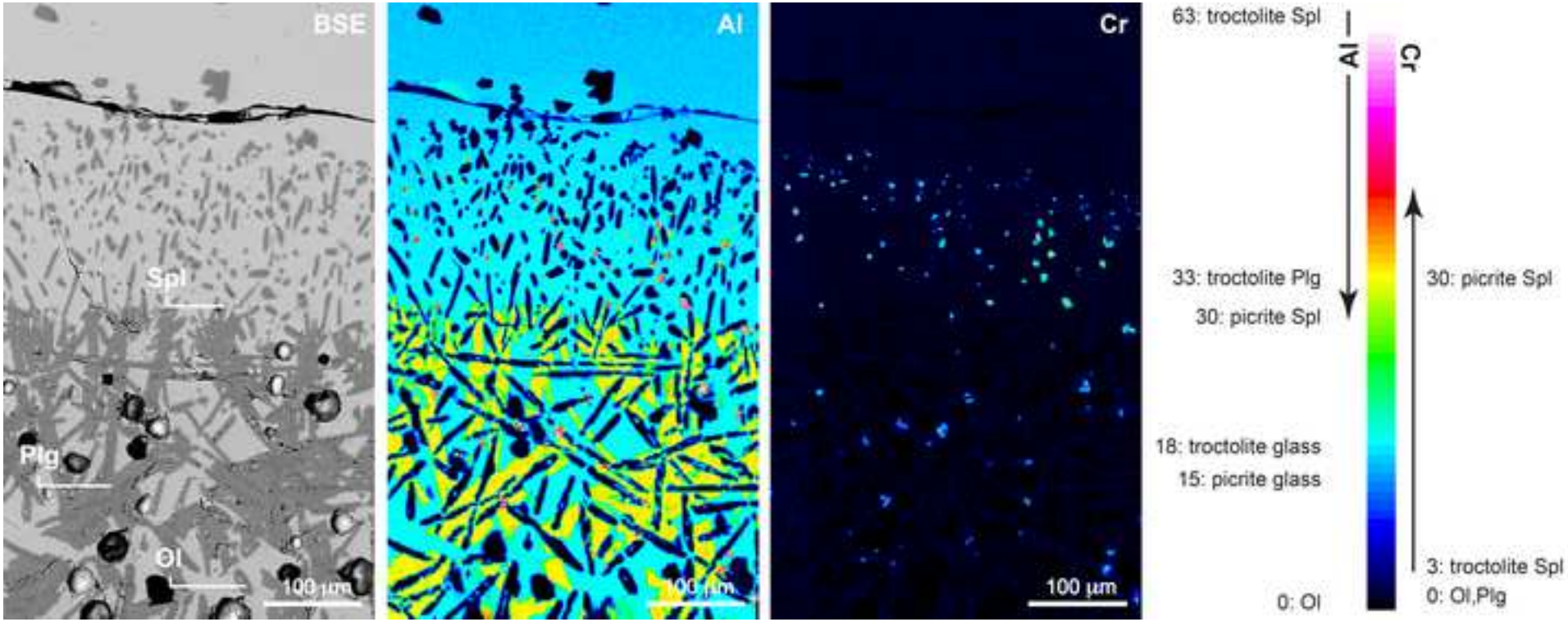

Figure10
Click here to download Figure: Fig10.eps

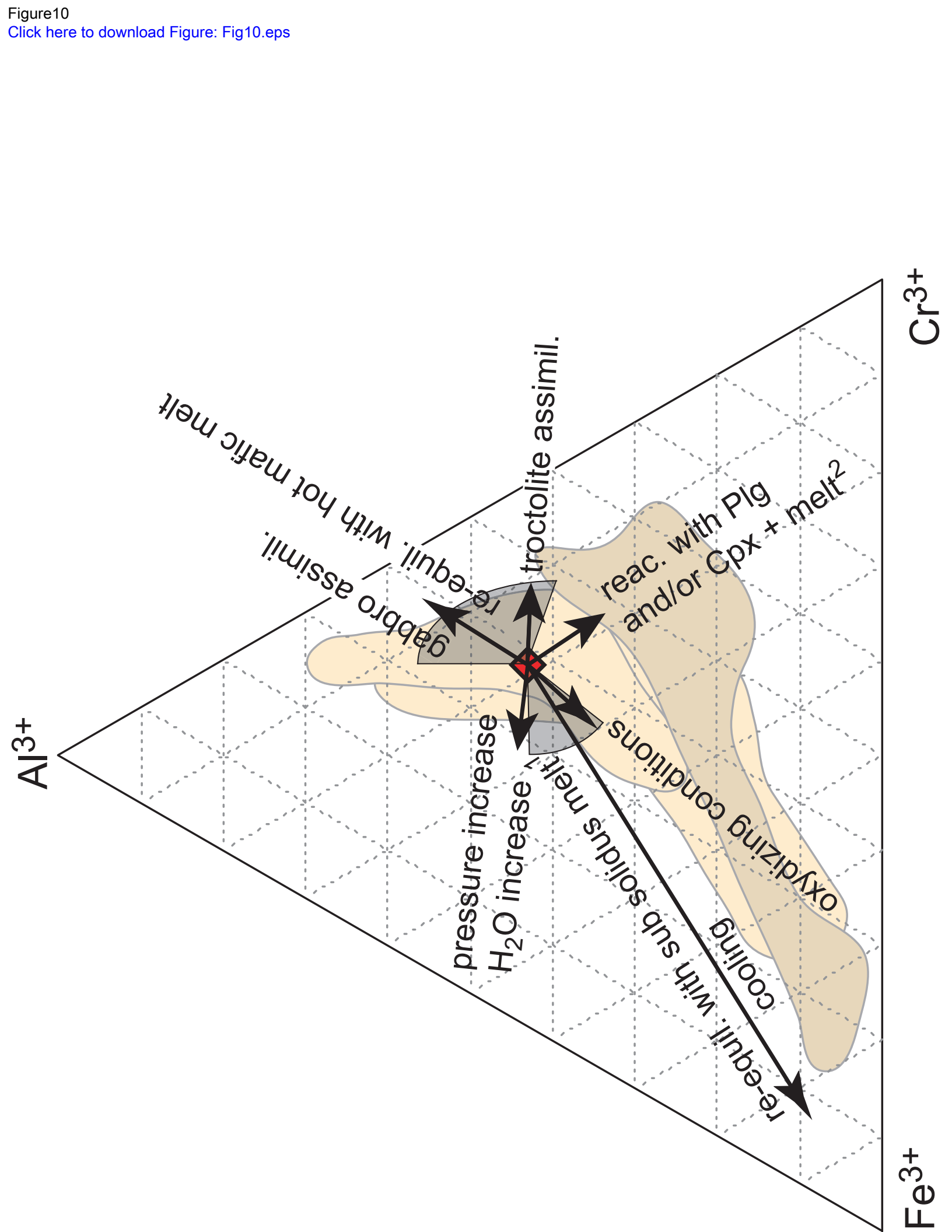

Table1
Click here to download Table: Table 1.doc

Table 1	Composition of starting materials (wt%)			
	picrite B62/2[a]	basalt 11JL33[b]	troctolite 11JL16[b]	gabbro 11JL27[b]
SiO_2	45.76	47.09	42.93	48.66
TiO_2	1.56	2.14	0.08	0.29
Al_2O_3	13.58	14.12	18.03	16.30
Cr_2O_3	0.11	0.03	0.09	0.10
Fe_2O_3	12.38	13.21	8.26	6.26
MnO	0.19	0.2	0.11	0.11
MgO	12.42	6.47	19.44	10.83
CaO	11.25	10.43	9.79	15.39
NiO	0.04	0.01	0.07	0.03
Na_2O	2.23	2.97	0.62	1.31
K_2O	0.16	0.57	0.02	0.02
P_2O_5	0.13	0.20	0.01	0.01
LOI	0.51	2.58	0.27	0.61
Total	100.32	100.04	99.72	99.92
Mg#[c]	0.67	0.49	0.82	0.77

[a] Upton et al. (2002)
[b] Leuthold et al (2014a)
[c] molar Mg#

Table2

Click here to download Table: Table 2.doc

Table 2. Gas mixing furnace experiments (1 atm, anhydrous) and run products

run#	Starting material conditions			Cooling mode	Final equilibration conditions			Phases identified and proportions				
	T [°C]	fO_2	duration [min]		T [°C]	fO_2	duration [hours]	Liq [%]	Ol [%]	Cr-spl [%]	Plg [%]	Cpx [%]
Experiments with B62/2 picrite												
61	1290	QFM	30	quenching	1180	QFM-2.2	5.5	x	x	<0.1	x	-
57	1290	QFM	30	quenching	1160	QFM-2.2	10.0	34	x	-	x	x
174					1360	QFM-1.2	0.4	100	-	-	-	-
135	1330	QFM-1.2	20	quenching	1240	QFM-1.2	2.5	90	10	0.1	-	-
136	1330	QFM-1.2	20	quenching, T oscillation	1200	QFM-1.2	3.5	x	x	x	-	-
137	1340	QFM-1.2	20	quenching, T oscillation	1190	QFM-1.2	3.3	83	11	0.2	6	-
161	1360	QFM-1.2	20	quenching, T oscillation	1175	QFM-1.2	6.5	x	x	x	x	x
114/1	1365	QFM	60	quenching, cooling from 1250°C, T oscillation	1165	QFM-1.2	69.0	61	11	<0.1	20	8
163	1360	QFM-1.2	20	quenching, T oscillation	1140	QFM-1.2	17.25	x	x	-	x	x
152	1350	QFM-1.2	20	quenching, cooling from 1190°C with T oscillation	1125	QFM-1.2	17.3	27	13	0.1	36	24
28					1320	QFM	0.5	100	-	-	-	-
98	1355	QFM	60	quenching	1280	QFM	9.5	97	3	x	-	-
62	1290	QFM	30	quenching	1260	QFM	1.0	96	4	0.1	-	-
60	1260	QFM	30	quenching, equilibration at 1170°C (60h, QFM), melting at 1260°C	1260'	QFM	0.5	x	x	x	-	-
107	1355	QFM	60	quenching	1230	QFM	5.0	x	x	x	-	-
106	1335	QFM	60	quenching	1210	QFM	8.3	x	x	x	-	-
87	1310	QFM	30	quenching	1210	QFM	11.3	x	x	x	-	-
47	1260	QFM	45	quenching	1210	QFM	7.0	90	9	x	-	-
48	1260	QFM	45	quenching	1200	QFM	16.3	95	4	0.1	1	-
49	1260	QFM	60	cooling	1190	QFM	8.3	89	11	0.2	-	-
53	1260	QFM	60	quenching	1180	QFM	15.0	68	14	0.1	18	1
30				partially molten powder	1180	QFM	5.0	x	x	x	x	x
51	1260	QFM	45	cooling	1170	QFM	19.0	64	17	0.1	12	7
54	1260	QFM	45	quenching	1160	QFM	16.8	x	x	x	23	x
56	1260	QFM	45	quenching, cooling from 1190°C with T oscillation	1160	QFM	20.0	46	20	0.1	21	12
27				partially molten powder	1160	QFM	16.0	x	x	x	x	x
88	1310	QFM	30	quenching	1150	QFM	13.5	x	x	x	x	x
55	1260	QFM	45	quenching	1140	QFM	6.5	x	x	x	30	x
52	1260	QFM	60	cooling	1140	QFM	22.0	39	14	0.1	34	13
63	1290	QFM	30	cooling	1125	QFM	21.0	30	14	0.1	37	19
105	1335	QFM	60	quenching, T oscillation	1110	QFM	91.0	4	16	2.2 (Spl)	46	31
165	1360	QFM+0.8	20	quenching, T oscillation	1140	QFM+0.8	17.0	x	x	x	x	x
166	1360	QFM+0.8	20	quenching, T oscillation	1125	QFM+0.8	14	x	x	x	x	x
59	1290	QFM	30	quenching	1190	QFM+1.8	10.5	x	x	x	x	-
99	1355	QFM	60	quenching	1180	QFM+1.8	12.5	x	x	lot	x	-
58	1290	QFM	45	quenching, cooling from 1185°C	1160	QFM+1.8	12.0	54	15	1.1	20	10

Table3

Click here to download Table: Table 3.doc

Table 3. Gas mixing furnace experiments (1 atm, anhydrous) and run products

run#	Starting material conditions			Cooling mode	Final equilibration conditions			Phases identified and proportions				
	T [°C]	fO_2	duration [min]		T [°C]	fO_2	duration [hours]	Liq [%]	Ol [%]	Cr-spl [%]	Plg [%]	Cpx [%]
Experiments with 11JL33 basalt												
176					1230	QFM-1.2	0.5	100	-	-	-	-
167	1235	QFM-1.2	30	quenching, T oscillation	1170	QFM-1.2	2.5	x	x	-	-	-
168	1235	QFM-1.2	30	quenching, T oscillation	1150	QFM-1.2	3.5	x	x	-	x	x
169	1235	QFM-1.2	30	quenching, T oscillation	1135	QFM-1.2	4.25	x	x	-	x	x
151	1210	QFM	20	quenching, cooling with T oscillation	1125	QFM-1.2	4.25	x	x	x	x	x
170	1235	QFM-1.2	30	quenching, T oscillation	1120	QFM-1.2	14	x	x	-	x	x
171	1235	QFM-1.2	30	quenching, cooling, T oscillation	1085	QFM-1.2	4.3	x	x	x	x	x
177					1210	QFM-0.7	0.4	100	-	-	-	-
132	1210	QFM-0.7	20	quenching	1150	QFM-0.7	3.5	x	x	x	x	±
133/2	1210	QFM-0.7	20	quenching, T oscillation	1135	QFM-0.7	3.5	x	x	x	x	x
133/1	1210	QFM-0.7	20	quenching	1130	QFM-0.7	3.5	x	x	x	x	x
134	1210	QFM-0.7	20	quenching, T oscillation	1150	QFM-0.7	3.5	x	x	x	x	x
110					1180	QFM		100	-	-	-	-
64	1290	QFM	45	quenching, cooling from 1230°C	1170	QFM	7.4	100	-	-	-	-
113	1230	QFM	15	cooling from 1230°C, T oscillation	1150	QFM	43	86	4	<0.1	10	-
70	1290	QFM	30	quenching, cooling from 1190°C	1125	QFM	19.1	x	x	<0.1	x	-
124	1215	QFM	0	cooling from 1215°C, T oscillation	1120	QFM	20	57	6	<0.1	30	7
71	1250	QFM	30	quenching, T oscillation	1090	QFM	67.3	33	3	7 (Spl)	38	19
129	1200	QFM	15	cooling with T oscillation	1085	QFM	117	x	x	x (Spl)	x	x
130	1200	QFM	20	quenching, T oscillation	1075	QFM	24	x	x	x (Spl)	x	x
131	1210	QFM	20	quenching, T oscillation	1060	QFM	50	2	3	5 (Spl)	53	37

Table4

Click here to download Table: Table 4.doc

Table 4. Gas mixing furnace experiments (1 atm, anhydrous) and run products

run#	Starting material conditions			Cooling mode	Final equilibration conditions			Phases identified and proportions				
	T [°C]	fO_2	duration [min]		T [°C]	fO_2	duration [hours]	Liq [%]	Ol [%]	Cr-spl [%]	Plg [%]	Cpx [%]
Experiments with 50:50 mix of B62/2 picrite + 11JL16 troctolite												
179					1370	QFM-1.2	0.4	96	4	-	-	-
97	1370	QFM	180	quenching	1200	QFM-1.2	16.3	x	x	x	x	-
149				partially molten powder	1190	QFM-1.2	43	x	x	x	x	-
146	1370	QFM-1.2	20	quenching, cooling from 1250°C, T oscillation	1180	QFM-1.2	48.0	31	24	0.1	45	-
96					1370	QFM	3.0	100	-	-	-	-
77	1460	air	30	quenching, T oscillation	1250	QFM	3.3	78	22	0.2	-	-
76	1320	QFM	30	quenching, T oscillation	1230	QFM	4	69	18	0	13	-
75	1320	QFM	20	quenching, T oscillation	1210	QFM	7.2	x	x	x	x	-
78	1460	air	15	quenching, T oscillation	1190	QFM	6.75	x	x	0	x	-
74	1320	QFM	30	quenching, T oscillation	1190	QFM	12.0	28	32	0.1	40	-
143	1370	QFM	20	quenching, cooling from 1250°C with T oscillation	1190	QFM	20.0	x	x	x	x	-
95	1370	QFM	180	quenching	1185	QFM	15.0	30	x	x	x	-
144	1370	QFM	180	quenching, cooling from 1260°C with T oscillation	1180	QFM	44.0	32	28	0.1	40	-
146	1370	QFM	180	quenching, cooling from 1250°C with T oscillation	1170	QFM	67.3	x	x	x	x	x
79	1460	air	15	quenching, T oscillation	1160	QFM	6.6	13	23	1.5	50	12
80	1460	air	15	quenching, cooling from 1170°C	1145	QFM	94.0	T < solidus				
180					1400	QFM+0.8	0.4	100	-	-	-	-
122/1	1360	QFM	60	quenching, T oscillation	1220	QFM+0.8	20.0	x	x	x	x	-
122/2				partially molten powder	1220	QFM+0.8	20.0	x	x	x	x	-
123	1360	QFM	60	quenching, T oscillation	1190	QFM+0.8	1.5	x	x	x	x	-
141	1400	QFM+0.8	20	quenching, T oscillation	1190	QFM+0.8	26.5	x	x	x	x	-
142	1400	QFM+0.8	20	quenching, cooling from 1260°C	1190	QFM+0.8	73.0	x	x	x	x	-
Experiments with 11JL16 troctolite												
153	1500	QFM-1.2	20	quenching				100	-	±	-	-
81	1500	air	15	quenching	1210	QFM	15.3	5	x	x	x	-

Table5

Click here to download Table: Table 5.doc

Table 5. Gas mixing furnace experiments (1 atm, anhydrous) and run products

run#	Starting material conditions			Cooling mode	Final equilibration conditions			Phases identified and proportions				
	T [°C]	fO_2	duration [min]		T [°C]	fO_2	duration [hours]	Liq [%]	Ol [%]	Cr-spl [%]	Plg [%]	Cpx [%]
Experiments with 50:50 mix of B62/2 picrite + 11JL27 gabbro												
173	1360	QFM	20	quenching, T oscillation	1190	QFM-1.2	42.0	x	x	x	x	x
115	1500	QFM	15	quenching	1290	QFM	1.5	100	-	-	-	-
86	1310	QFM	45	quenching	1235	QFM	4.1	98	2	0.1	-	-
73	1320	QFM	30	quenching, T oscillation	1225	QFM	3.8	97	2	0.1	1	-
69	1290	QFM	45	quenching, cooling from1250°C	1210	QFM	5.7	x	x	x	x	-
68	1290	QFM	45	quenching, cooling from1230°C	1190	QFM	8.8	70	9	0	19	2
85	1310	QFM	45	quenching, T oscillation	1170	QFM	16.75	33	9	0	35	23
116	1500	QFM	15	quenching, T oscillation	1165	QFM	51.0	x	x	x	x	x
66	1290	QFM	45	cooling	1140	QFM	10.3	20	7	0.1	42	31
Experiments with 11JL27 gabbro												
181	1350	QFM-1.2	20	quenching, cooling from 1240°C, T oscillation	1190	QFM-1.2	15	x	x	x	x	x
182	1350	QFM-1.2	20	quenching, cooling from 1240°C, T oscillation	1170	QFM-1.2	37.0	x	x	x	x	x
83	1290	QFM	60	quenching	1230	QFM	2.0	98	1	0.1	1	-
108	1355	QFM	60	quenching, cooling from 1240°C with T oscillation	1210	QFM	15.0	x	x	x	x	x
72	1320	QFM	30	quenching, T oscillation	1210	QFM	17.5	x	x	x	x	x
94	1295	QFM	55	quenching, cooling from 1210°C, T oscillation	1190	QFM	1	30	x	x	x	x
65	1290	QFM	45	quenching, cooling from 1230°C	1170	QFM	6.5	25	7	<0.1	48	20

Appendix Figure 1

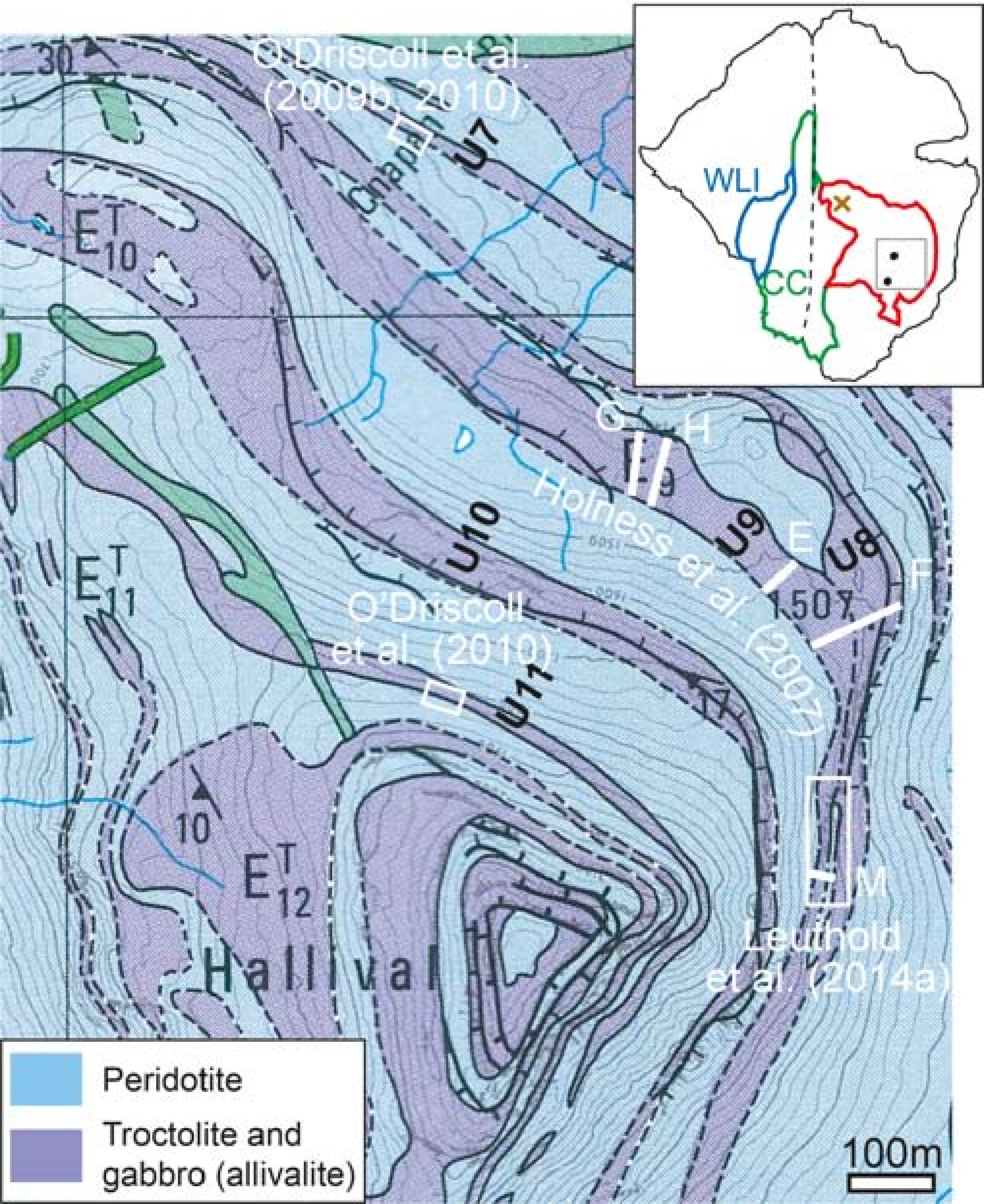

Appendix Figure 2

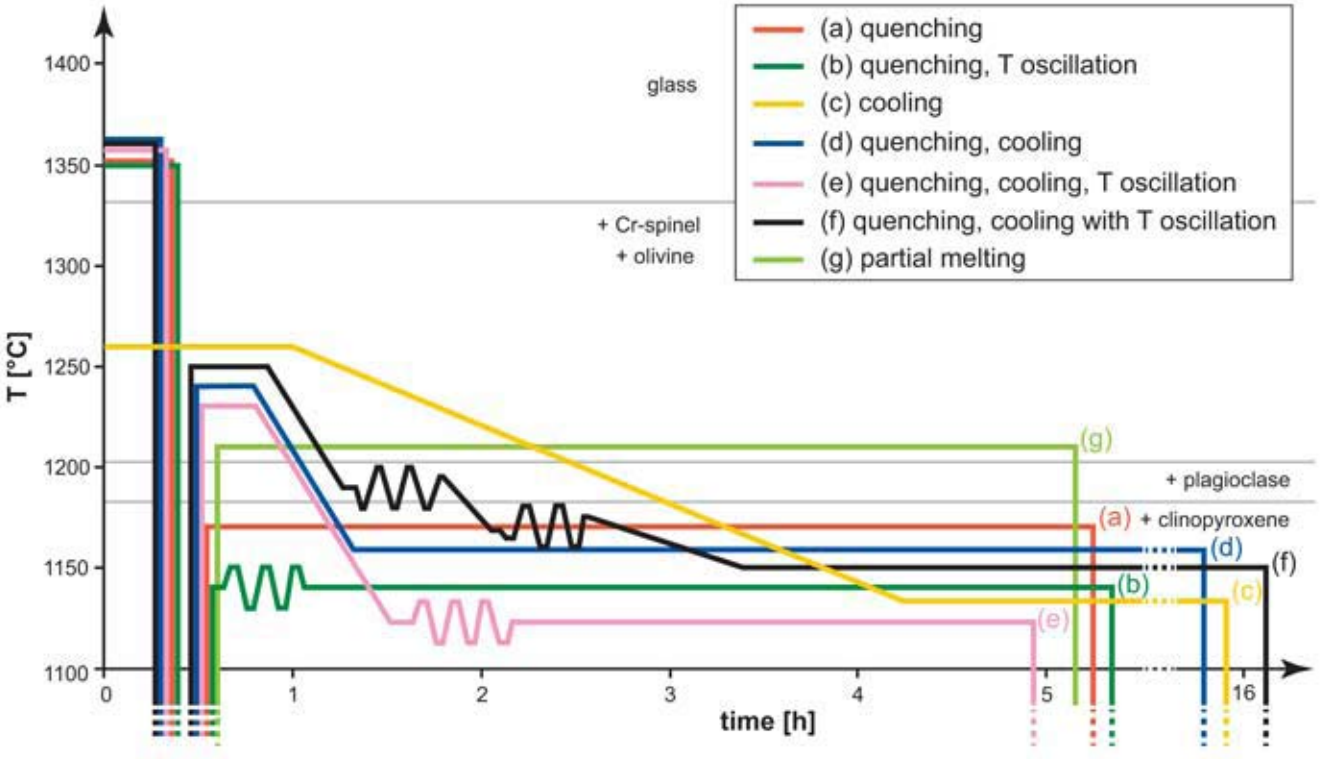

Appendix Figure 3

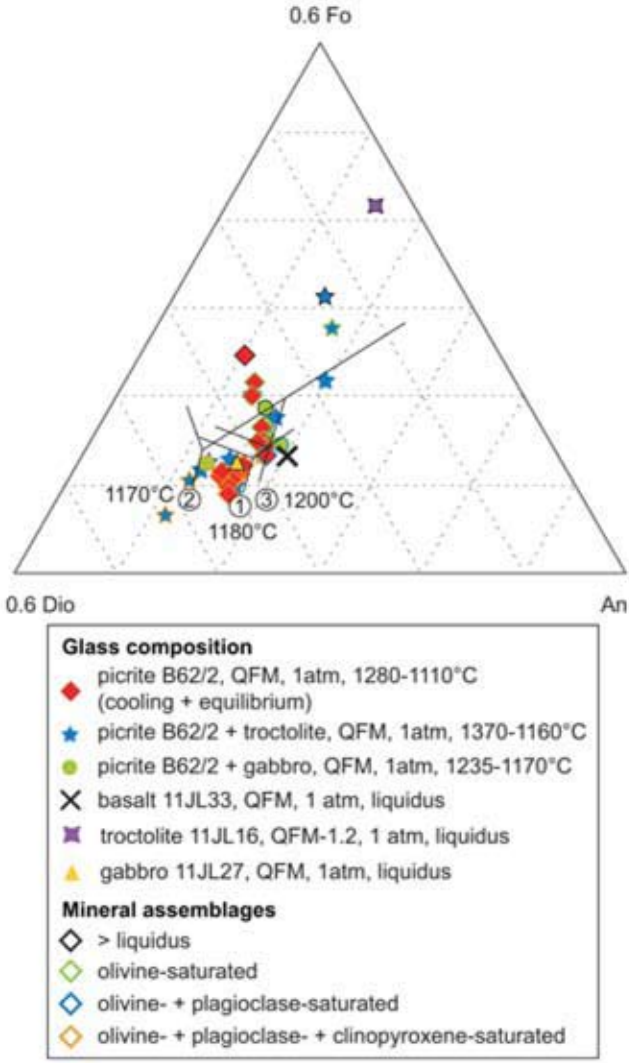

The online version of this article (doi:10.1007/s00410-015-1165-0) contains supplementary material, 4-6 (Appeddix Tables 1-3)